Alma Mater Studiorum · University of Bologna

School of Science
Department of Physics and Astronomy
Master Degree in Physics

Baryogenesis from Phase Transitions below a GeV

Supervisor:
Dr. Filippo Sala

Co-supervisor:
Prof. Silvia Pascoli

Submitted by:
Alessia Musumeci

Academic Year 2023/2024

Abstract

The aim of the thesis is to build a baryogenesis model from a First Order Phase Transitions (FOPTs) below a GeV, producing gravitational waves that could explain those recently observed by Pulsar Timing Arrays. Baryogenesis models aim to solve one of the open problems of the Standard Model, namely the asymmetry between matter and antimatter observed in the Universe. In the last decades, many new physics models have been proposed to address this question, motivated by theoretical considerations and experimental opportunities. In particular, in this work, we consider a baryogenesis mechanism where a fermionic dark matter candidate and a neutron mix via an effective operator and the baryon asymmetry is produced at cosmological temperatures of $\mathcal{O}(10)\,\mathrm{MeV}$ via resonant oscillations between neutron and dark matter. This idea can be implemented in a model with a dark $U(1)'$ gauge symmetry where the mass of the associated "dark" photon is generated via a "dark" Higgs mechanism. The main novelty of this work is that we assume that the potential of the dark Higgs scalar is scale invariant and that its vacuum expectation value (VEV) is generated by radiative corrections at one-loop, as in the Coleman-Weinberg model. The VEV enters in the mass mixing term and, ultimately, in the baryon asymmetry. This effective potential at one loop induces a supercool FOPT and lead to the generation of Gravitational Waves (GWs). We find that the parameters of our model yielding to successful baryogenesis could also explain the recent GWs observation at Pulsar Timing Arrays.

Contents

Chapter 1

Introduction

The Standard Model (SM) of Particle Physics is the current theoretical framework that describes nature at the smallest scales. Despite its history of successes, which culminated in the discovery of the Higgs boson in 2012 [1, 2], we know that it is not a complete theory. Indeed, on top of theoretical issues, such as the hierarchy problem or the strong CP problem, as of today, several independent experiments and observations imply that physics beyond the SM (BSM) is needed to explain:

- the neutrino masses
- the baryon asymmetry of the Universe
- the existence of Dark Matter

In this thesis we are mainly concerned with the second open problem, that goes under the name of *matter-antimatter asymmetry problem*. The theories that aim to solve this problem are called theories of *baryogenesis*.

Initially, the value of the baryon asymmetry was considered as one on the fundamental parameters of the Big Bang model, however, this is incompatible with the inflationary paradigm, which is the only known solution to the horizon and flatness problems of our cosmological model, see e.g. [3]. However, and moreover, in 1967, Sakharov pointed out [4] that it was possible to generate a baryon asymmetry dynamically during the evolution of the Universe, which is more appealing than fixing an initial parameter, and most importantly is compatible with inflation. Since then, there has been a great effort in formulating possible mechanisms to generate the baryon asymmetry and, even now, particle theorists come up with many new models (see e.g. [5, 6] for recent reviews), motivated by either new theoretical ideas or possible experimental opportunities. We will discuss theories of baryogenesis in detail in Chapter 2.

Probing these theories remains a non trivial point since many of the mainstream baryogenesis invoke new physics above the TeV scale and hence are very difficult to test. Nevertheless, there are many new paradigms that predict new physics at low scales. In the next decade, their associated experimental signatures could show up , for example, in $n - \bar{n}$ oscillations, flavour observables, searches for the permanent electric dipole moment, neutrinoless double beta decay, gravitational waves interferometers, underground experiments, as well as next generation colliders [6].

In particular, Gravitational Waves (GW) offer us a new way to look at the Universe and, in the recent years, especially after the the first direct detecton of the Gravitational Wave Signal by the LIGO interferometer in 2015 [7], we had an impressive development in this field of research, both on the experimental and the theoretical side. GWs can be produced by many astrophysical objects, but, in particular, a Stochastic Gravitational Wave Background (SGWB) could be sourced by Cosmological First Order Phase Transitions (FOPTs). In the SM there are no FOPTs (see later Section 3.1), but they are predicted in many BSM theories, hence making the GWs observations a complementary probe for fundamental physics.

The idea of connecting baryogenesis models with FOPTs, and hence, a possible detectable GW signal has been already extensively studied in literature. Firstly, in the context of Electroweak Baryogenesis (see Section 2.5.1 for a brief description), which, in order to work, requires a first order phase transition at the electroweak scale ($T \sim 100$ GeV). In particular realisations of EWBG, the PT can lead to the generation of a SGWB detectable by the LISA interferometer (For recent developments, we refer to Ref. [8]). Other non-traditonal baryogenesis mechanics have been proposed in Refs. [9, 10, 11, 12] where the baryon asymmetry can obtained via out-of-equilibrium decays of heavy particles that are produced in a FOPT. Some realizations of these mechanisms are expected to produce a SGWB in future interferometers, such as LISA, DECIGO and Einstein Telescope. Nevertheless, as of today, it has never been proposed a testable baryogenesis mechanism that is testable in one class of running experiments looking for a SGWB, which are particularly interesting because they recently reported the observation of a SGWB: the Pulsar Timing Arrays (PTAs) observatories.

What are PTAs? As the name suggests, the main astrophysical object of interest is a pulsar. A pulsar is a rapidly rotating magnetized neutron star which emits electromagnetic radiation along the rotating axis, like a lighthouse. The rotation frequency of the axis is linked to the rotation of the pulsar, which is very stable because of the conservation of angular momentum. Therefore, the light pulses arrive in regular intervals and they can be used as clocks (for more details on timing pulsars and more general aspects on pulsars, see e.g. Ref. [13]). It was

discovered that millisecond pulsars are very stable in their rotation, with a timing precision close to atomic clocks [14]. The series of pulses emitted by pulsars are regularly observed by radio telescopes. We define a *pulsar timing residual* as the difference between the expected time of arrival and the observed time of arrival of light from pulsar. The time of arrival encodes information about the propagation of radio waves, including interstellar medium effects and spacetime deformation due to GWs. The effect of GWs is very weak, but one can identify a pattern in the pulsar residual data from all the pulsars [15]. If a SGWB is indeed present, the relation between the correlation of two pulsars and their angular separation has a particular shape, which is known in literature as the Hellings-Downs curve.

In the recent years, PTAs have gained a lot of attention since the collaborations NANOGrav [16], PPTA [17], EPTA [18] and IPTA [19] have gained evidence for the existence of a SGWB. A possible astrophysical explanation of the signal is the production of GWs from the merging of Supermassive Black Hole Binaries (see, for example, Ref. [20]), but many different explanations that invoke the existence of New Physics beyond the SM have been proposed, such as cosmological FOPTs [21], cosmic strings [22], domain walls [23], axion dynamics [24, 25] or large scalar fluctations (see e.g. Ref. [26]). In particular, for the PTAs frequency range, a FOPTs has to occur at a scale below the GeV, because of causality constraints [27].
As we have previously stated, as of today, there is no explanation of the PTAs signal that is connected with the generation of the baryon asymmetry. Therefore, the goal of this thesis is to find a baryogenesis model from a FOPTs below a GeV that could explain the observed PTAs signal.

This thesis is organized as follows. In Chapter 2 we will discuss the matter-antimatter problem in more detail, describing its experimental evidence and why the current Standard Cosmological Model and the SM fail to give an explanation for it. Hence, we will present old and new ideas to solve this problem. In Chapter 3 we will introduce First Order Phase Transitions, giving a brief overview on the theoretical tools to describe their dynamics. In particular, we will introduce the parameters that enter in the prediction of the GW spectrum. We will then compute one of these parameters, namely the nucleation temperature, in two different BSM scenarios. We will also introduce supercooled phase transitions. In Chapter 4 we will discuss our proposal of baryogenesis from a weakly-coupled supercooled phase transition below the GeV scale, where the baryon asymmetry is generated via the resonant oscillations between dark matter and neutrons. In Chapter 5 we conclude.

Chapter 2

Baryogenesis: motivations and models

2.1 Evidence for the Baryon Asymmetry of the Universe

The existence of antimatter was first predicted by Paul Dirac as a consequence of the combination between the theory of special relativity and quantum mechanics [28] and then discovered by Carl Anderson [29]. After its discovery, antimatter was thought to be an exact mirror of matter [30]; all phenomena that had been observed in Nature were invariant under the conjugation of parity (P) and charge (C) as well as time reversal (T) and thus, in principle, there is nothing that prevents antimatter to form the same "complex" structures that we observe in the Universe, such as stars, galaxies, etc., and yet there is no sight of them around us. In this Section, we will explain how we came to the conclusion that we live in a matter dominated Universe.

To begin with, our Earth is definitely not made of antimatter, as well as many other planets of our Solar System that we were able to reach with spacecrafts. The Sun is also made of matter as proven by solar winds. Solar winds provide a strong argument for the matter-antimatter asymmetry in our Solar System. In fact, if the planets and satellites were made of antimatter, this outflow of particles from the Sun could reach their surface (the possible deflection from magnetic fields around the planets doesn't ruin this argument since there could be places, such as the magnetic poles, where the solar wind particles can leak in [31]) and the annihilation of the solar winds on their surfaces would make them the strongest γ-ray sources [32].

If we look at other parts of the galaxy, a direct probe comes from the measure-

ments of antiprotons and protons in cosmic rays, which have been studied by the PAMELA and FERMI space observatories [30]. It was discovered that the fraction of protons and antiprotons is consistent with a Universe that is entirely made of matter and this fraction can be simply explained by pair production in astrophysical processes [30]. As of today, there is no discovery of heavier antinucleids, which would indicate the existence of antimatter within our galaxy, as confirmed by the lack of finding by the Alpha Magnetic Spectrometer (AMS) [33].

Indirect probes of the matter domination in other galaxies come from the observation of γ rays from annihilation processes, since, through $p\bar{p}$ annihilations into pions and the subsequent decay of the π^0 into γ rays, we should be able to see the interface between the matter dominated region and the antimatter dominated region in the diffuse γ-ray background [30, 34, 35]. If we look at even larger scales, the X-rays observations from colliding clusters allow us to infer an upper bound on the fraction of antimatter in galaxy clusters. From the observations of the colliding clusters that constitute the Bullet Cluster, it was found that, if there are regions of antimatter in the Universe, they must be separated from regions of matter by distances of the order of tens of Mpc, i.e. the size of the galaxy cluster itself.

We have a last possibility to discuss. Is the Universe a patchwork of regions that are strongly dominated by either matter or antimatter? The answer is no because, if this were the case, the size of these regions would be at least comparable with the size of the Universe, as probed by the measured cosmic diffuse γ-ray background [34, 35].

2.2 Measuring the Baryon Asymmetry

We have collected enough evidence that tells us that we live in a Universe that is matter dominated and therefore we can now concern ourselves with the measurement of this asymmetry.
The baryon asymmetry can be parameterized in different ways. Here we will define the baryon asymmetry η_B as the difference between the number density of baryons n_b and the number density of anti-baryons $n_{\bar{b}}$ divided by the number density of photons n_γ, since the end products of annihilation processes are mainly photons. Hence we obtain:

$$\eta_B = \frac{n_B - n_{\bar{B}}}{n_\gamma} \approx \frac{n_B}{n_\gamma} \tag{2.1}$$

where the last approximation is consequence of the discussion of the previous section, i.e. we have a negligible amount of antimatter in the Universe. Moreover, we point out that the baryons are mainly protons and ^{4}He after the CMB.

This way to express the baryon asymmetry is particular convenient since the baryon number density is not constant during the evolution of the Universe, but it scales like a^{-3}, where a is the cosmological scale factor.
This parameter can be measured in two independent ways [30].

- **Big Bang Nucleosynthesis** The Big Bang Nucleosynthesis (BBN) happens when protons and neutrons combine together, leading to the production of deuterium (D), helium (^{3}He,^{4} He) and lithium (^{7}Li). BBN starts around 1 MeV, when the neutrinos go out of the equilibrium with the thermal plasma. At this scale, well understood SM physics come into play, therefore making BBN a reliable probe of the Early Universe physics. In this case, the only unknown parameters that enters in BBN is η_B, which the predictions of the abundances of the light elements produced during BBN will depend on. Assuming that we are within the standard scenario where the effective number of neutrino species is $N_\nu = 3$ and by fitting the data for the primordial abundances, the estimate for the baryon-to-photon ratio is [36]:

  $$\eta_B = (5.931 \pm 0.051) \times 10^{-10} \tag{2.2}$$

  The uncertainties in the result derive from the measurements of the primordial elements, but it is important to notice that η_B is mainly sensitive to the abundance of D, thus avoiding complications from the the known *lithium problem* [37].

- **Cosmic Microwave Background** The baryon asymmetry has been determined from the angular power spectrum of temperature fluctuations in the Cosmic Microwave Background (CMB). The variation in the temperature were generated by acoustic oscillations of the baryon-photon plasma in the gravitational potential due to the small inhomogeneities in the Dark Matter distribution [30]. The dependence of η_B enters in the equation of state of the plasma and decreasing η_B would lead to larger ratio between the peaks of the spectrum. Using the results from PLANCK, the estimate for the baryon-to-photon ratio reads [38]:

  $$\eta_B = (6.12 \pm 0.04) \times 10^{-10} \tag{2.3}$$

2.3 The Baryon Asymmetry and Cosmology

In this section we will investigate possible origins for the observed baryon asymmetry.

2.3.1 Baryon Asymmetry and Inflation

A first, simple approach to the matter-antimatter problem would be arguing that the baryon asymmetry is an initial condition of our Universe, however this idea is in conflict with the now widely accepted inflationary paradigm, which provide an explanation to the observed flatness, isotropy and homogeneity of the Universe (see [39] for a recent review on inflaton). In this scenario, during the evolution of the Early Universe, the energy density is dominated by the vacuum energy of a scalar field, called the inflation, and the comoving scales grow quasi-exponentially. At the end of inflation, the Universe is in a cold, low entropy state with a few degrees of freedom and the the inflaton energy density is then converted into radiation in a process called reheating. Therefore, at the end of inflation, the Universe does not contain any matter and it is perfectly baryonic symmetric. If indeed there was an initial baryon asymmetry, we would have to squeeze the baryons in a small patch, their energy density would be larger than the one of the inflaton and it would lead to an estimate of the Hubble parameter that is very different from the one that we observe in experiments [3, 40].

2.3.2 Baryon Asymmetry and BBN

We have come to the conclusion that the baryon asymmetry must be generated after inflation. Therefore, let us now start with $\eta = 0$. Can we explain the observed baryon asymmetry within the Standard Cosmological Model? The equilibrium abundance of baryons b and antibaryons $\bar{b}$ at $T \lesssim 1$ GeV, i.e. in the non-relativistic regime, is:

$$\frac{n_b}{n_\gamma} \simeq \frac{n_{\bar{b}}}{n_\gamma} \simeq \left(\frac{m_p}{T}\right)^{3/2} e^{-\frac{m_p}{T}} \tag{2.4}$$

with m_p the mass of the proton. As the temperature decreases, if the annihilation rate Γ_{ann} is larger than the expansion rate of the Universe H, the number of nucleons and anti-nucleons decreases. When $T \simeq 20$ MeV, $\Gamma_{\text{ann}} \simeq H$ and annihilations freezes out. Therefore, we obtain from Eq.(2.4):

$$\frac{n_b}{n_\gamma} \simeq \frac{n_{\bar{b}}}{n_\gamma} \simeq 10^{-18} \tag{2.5}$$

However, this number is much smaller than the one that is required by the Big Bang Nucleosynthesis. A possible solution may be introducing new interactions that separate matter from antimatter when $\eta \sim 10^{-10}$ at temperatures smaller than 38 MeV. However, at this time scale, we can't explain the asymmetry over the galaxy scales, because of causality. This scenario is not valid in cosmological models with an inflationary period, but yet again, if separation occurs after inflation, it is not clear how causality would lead to the generation of such an asymmetry. Another

possible solution could be a statistical fluctuation in the baryon and antibaryon distributions, but it would lead to a value which is again much smaller than the observed baryon asymmetry [3].

In conclusion, in the standard cosmological model there is no explanation for such a small value of the baryon asymmetry consistent with nucleosynthesis. A primordial asymmetry could be put by hand, but it is not a satisfactory solution since we want to write down a fundamental theory that predicts its value. Moreover, if we accept the inflationary paradigm, the baryon asymmetry must be generated some time after the era of inflation and any upper limit on the reheating temperature constrains the possible mechanisms for baryogenesis.

2.4 The Baryon Asymmetry and the Standard Model

2.4.1 Sakharov conditions

As already anticipated in the Introduction, in 1967, after the discovery of CP violation in K^0 [41], A.D. Sakharov proposed in his seminal paper on baryogenesis [4] three necessary conditions, known as *Sakharov conditions*, for the generation of matter-antimatter asymmetry from a particle physics model:

1. **Baryon-number violation** Since the Universe is initially baryon symmetric ($B = 0$), then there need to be baryon number violating interactions that lead to a Universe with $B \neq 0$.

2. **C and CP violation** If C and CP were exact symmetries of fundamental interactions, the reaction rate of production of baryons would be balanced by the reactions that produce anti-baryons. Hence, a baryon asymmetry can't be generated.

3. **Departure from thermal equilibrium** If all the particles in the Universe remained in thermal equilibrium, then no preferred direction for time may be defined and the CPT invariance would prevent the appearance of any baryon excess, since any reaction would be proceed at the same rate as the inverse one, making the presence of CP violating interactions irrelevant.

2.4.2 Sakharov conditions in the Standard Model

At this point we my ask ourselves if the SM satisfies the Sakharov conditions. Let's look at each one of them in detail.

1. In the SM the baryon number and the lepton numbers, i.e. the three lepton numbers of each flavour are conserved at tree level. More precisely, each one

of them is the conserved charge of an accidental global $U(1)$ symmetry, where by *accidental* we mean that they happen to be symmetries of the Lagrangian because of the gauge group which defines the SM, but, if taken separately, they are anomalous, since they are violated by the triangle anomaly. We notice that the baryonic and leptonic currents J_B^μ and J_L^μ, at the non perturbative level, are not conserved, but they satisfy the following equation [42]:

$$\partial_\mu J_B^\mu = \partial_\mu J_L^\mu = \frac{n_f}{32\pi^2}(-g^2 W_{\mu\nu}^a \tilde{W}^{a,\mu\nu} + g'^2 B_{\mu\nu}\tilde{B}^{\mu\nu}) \tag{2.6}$$

where $g, W_{\mu\nu}, \tilde{W_{\mu\nu}}$ and $g', B_{\mu\nu}, \tilde{B}_{\mu\nu}$ are the gauge coupling, the field strenght tensor and the dual field strenght tensor of the the $SU(2)_L$ and $U(1)_Y$ symmetries of the SM, respectively, and n_f is the number of fermionic families ($n_f = 3$).

In the bosonic sector of the Electroweak theory within the SM, there is an infinite number of field configurations that minimise the static energy functional of the guage-Higgs fields, which we call *vacua*. They are physically equivalent, but they can be distingued by their Chern-Simons number N_{CS}. The change in the baryon number is related to the dynamics of the gauge fields:

$$B(t) - B(0) = n_f[N_{CS}(t) - N_{CS}(0)] \tag{2.7}$$

These are non-perturbative effect, given by the *sphaleron*, which is a static (time-dependent) solution to the electroweak field equations. Therefore, a transition between two different vacua implies a change of the baryon (lepton) number. It was showed that the transition via tunnelling is strongly suppresses at zero temperature, however, at high temperatures, the sphaleron transition are in thermal equilibrium [43]. More precisely:

$$\Gamma_{sph} = \begin{cases} \frac{E_{sp}}{T}\frac{m_W}{T}\, T^4\, e^{-\frac{E_{sp}}{T}} & T \lesssim 130\,\text{GeV} \\ 30\alpha_w^5\, T^4 & T \gtrsim 130\,\text{GeV} \end{cases} \tag{2.8}$$

where $\alpha_W = g^2/4\pi$ and E_{sp} is the height of the barrier between the two vacua. Hence, when $T \gtrsim 130\,\text{GeV}$, $B - L \neq 0$ is conserved and $B + L$ is violated.

For more details on sphaleron effects, one can read the review [44].

2. C is violated by the weak interactions and CP is violated by the CKM mechanism

3. The out-of-equilibrium condition can be satisfied if the $SU(2)_L \times U(1)_Y$ phase transitions, which is called the Electroweak Phase Transition (EWPT), is of

the first order, thus requiring that the mass of the Higgs boson must be smaller than 70 GeV [45, 46, 47]

However, quantitatively, the second and the third Sakharov conditions are not satisfied because of the measurements of the free parameters of the SM. In fact:

2. It was showed in Ref. [48, 49] that the CP effects are very much below what is required to solve the baryon asymmetry. A simple way to estimate the amount of CP-violation is to compute reparemetrisation invariant objects out of the quark mass matrices [30, 50]. The first CP violating quantity reads [51]:
$$\mathrm{Im}\left[\det[M_u M_u^\dagger, M_d M_d^\dagger]\right] \approx -2J\, m_t^4 m_b^4 m_c^2 m_s^2 \tag{2.9}$$
where $M_{u,d}$ are the mass matrices of up and down-type quarks, m_i are the mass eigenvalues of the quarks of flavour i and J is the Jarlskog invariant, which is defined as follows:
$$J = \mathrm{Im}[V_{us} V_{cb} V_{ub}^* V_{cs}^*] \tag{2.10}$$
with V_{ij} are matrix elements of the CKM matrix. A dimensionless quantity can be constructed when we divide by a relevant temperature to the 12^{th} power. If we take $T \approx 130$ GeV, at which the baryon asymmetry freezes out, we obtain the following estimate [50]:
$$\frac{J\, m_t^4 m_b^4 m_c^2 m_s^2}{T^{12}} \approx 10^{-19} \ll \eta_B \tag{2.11}$$

3. The mass of the Higgs m_H is too heavy ($m_H = 125\,\mathrm{GeV}$) for the EWPT to be of the first order, leading instead to a second-order phase transition or *crossover* (see e.g. Ref. [45]). As a consequence, the plasma remains too close to thermal equilibrium, the interactions between particles are fast and therefore very effective in suppressing any deviation from equilibrium due to the expansion of the Universe.

We conclude that the SM, as a quantum field theory, satisfies the Sakharov's conditions and thus, in principle, it can provide a possible (and economical) solution to the baryon asymmetry puzzle, however the experimental measurements show that it fails short quantitatively.

2.5 Baryogenesis: models and experimental tests

2.5.1 Main proposals for baryogenesis

We are now convinced of the fact that we need new physics in order to generate the baryon asymmetry and, indeed, particle theorists, following Sakharov's criteria,

have proposed a plethora of BSM models for baryogenesis. In this section we will review some of the most popular baryogenesis ideas that have been explored in the last decades [44, 52].

GUT baryogenesis Historically, the first models of baryogenesis were developed in the context of Grand Unified Theories (GUT) [1]. In GUT models the gauge groups of the strong, weak and electromagnetic interaction are united in a single gauge group, leading to a violation of the baryon number already at the perturbative level, see e.g. Ref. [54]. In these models the baryon asymmetry can generated from the decay of a heavy particle X with a mass comparable to the GUT scale $M_X \sim 10^{16}$ GeV. However, these models suffer from severe problems (see Ref. [55] for a brief summary), but the main one is due to inflation, since, in many inflationary models, the reheating temperature is well below the GUT scale.

Electroweak Baryogenesis We have seen in the previous section that in the Standard Model the EWPT can't provide a viable baryogenesis mechanism. However we can make the EWPT of the first order and we can have additional CP violating contributions by adding new physics ingredients. This class of baryogenesis goes under the name of Electroweak Baryogenesis models. These models are severely constraint by the measurements in the Higgs sector at LHC and by measurements of the electric dipole moment. However, there are some proposals that evade these bounds, for example in the context of Composite Higgs scenarios [56] or by considering time-varying Yukawa couplings [57, 58]. For a review on Electroweak Baryogenesis, we refer the reader to Ref. [44].

Leptogenesis This mechanism was first proposed by M. Fukugita and T. Yanagida in Ref. [59]. In this type of models a lepton asymmetry is generated by C, CP and lepton number violating processes involving a right-handed Majorana neutrino. The lepton asymmetry is then converted into the baryon asymmetry by sphaleron processes. Since the original proposal, many variants have been studied. For a brief review of these models, see Ref. [60].

2.5.2 Low scale baryogenesis

Most of the popular models predict that the baryon asymmetry is produced at very high temperatures, above or around the weak scale. However, in principle, it is possible to achieve baryogenesis at much lower scale, around 1-100 MeV. Indeed, this scenario emerges as a natural consequence in theories where the reheating

[1] Actually these first attempts were done without any input from Sakharov's paper, for more historical details see Ref. [53]

temperature is preferred at this low scale. For example, this scenario is predicted in some supersymmetric models (see e.g. Ref. [61, 62, 63]), in models of axion dark matter, where the low inflation scale implies a suppression of isocurvature perturbations (see e.g. Ref. [64]) and in models of dynamic relaxation of the weak scale [65]. The first proposals for low scale baryogenesis mechanism have been formulated in the 1980s [66, 67], in which, however, the baryon asymmetry actually gets diluted away by the decays of long lived heavy particles. Additionally, these models require large CP violations, on which we have severe constraints from electic dipole moments of particles [5].
Here we want to give a brief summary of a couple of promising low scale baryogenesis models that have been proposed in the last decade [5], while in Chapter 4 we will focus on a particular baryogenesis model, proposed in Ref. [68], that relies on the resonant oscillations between dark matter and neutron and it can produce the baryon asymmetry at the $\mathcal{O}(10)$ MeV scale. This model will be the starting point for our original proposal on baryogenesis from a supercooled FOPT.

Baryogenesis via Mesino Oscillations In Ref. [69] it was proposed a mechanism for baryogenesis at the 1-200 MeV scale. Starting from an extension of the SM (for example supersymmetric theories), they considered the particle-antiparticle oscillations of mesinos, which are bound states of a fermion quark and a scalar antiquark or viceversa. CP violations in these oscillations is possible and it could lead to the generation of the baryon asymmetry if there is a scalar quark such that:

- it lives long enough to hadronize
- it has baryon-number violating decays
- it is produced out of thermal equilibrium in the Early Universe

This model can be experimentally tested by finding evidence for scalar quarks at LHC.

Mesogenesis In a series of works [70, 71, 72] it was proposed a possible MeV-scale baryogenesis and dark matter production, which uses the CP violation processes of SM mesons, although CP violation contributions can also come from new physics sources. The generic mechanism proceeds as follows. We have a scalar field, with mass 10-100 GeV which decays at T_R, where $T_{\rm BBN} \lesssim T_R \lesssim T_{\rm QCD}$, to $q\bar{q}$ pairs, which then hadronize in charged or neutral mesons, which then undergo CP violating processes, such as neutral $B^0_{d,s}$ oscillations or charged meson decays. Moreover, we consider the existence of a dark sector, which allows us to infer that

actually the baryon number is never violated thanks to the introduction of a dark state ψ_B which carries baryon number $B = -1$.

We can divide the Mesogenesis models in two sub-classes. In the first one, an equal and opposite baryon asymmetry between the visible sector and the dark sector is generated, while in the second one a lepton asymmetry is generated and the converted to a baryon asymmetry between the two sectors via dark-sector processes.
This model can be tested in several expemeriments by measuring CP violating observables at B factories and at LHC, by finding evidence of decays of hadrons to dark baryons or in peak searches at colliders.

Chapter 3

First Order Cosmological Phase Transitions

3.1 Introduction

As of today, the Standard Model (SM) is the best framework to describe fundamental interactions, but both experimental evidence and theoretical arguments point out that the SM is not the final theory. One of its most studied phenomena is the nature of the electroweak phase transition and its possible consequences. Today the electroweak symmetry appears to be broken, however it was observed that in the Early Universe, at high temperature, the Higgs mass acquires thermal corrections and the minimum of the Higgs potential sits at the origin such that the electroweak symmetry is restored [73]. When the Universe expands, it cools down and then the true minimum is formed, the Higgs gets a vacuum expectation value and the symmetry gets broken. There is a phase transition from a symmetric to a broken phase.
In the SM the electroweak phase transition is of second order (or a *cross-over*) [45, 46, 47], as well as the QCD phase transition [74]. On the other hand, many models beyond SM make this transition a *first-order phase transition*, where the decay of the false vacuum to the true vacuum happens via bubble nucleation. The tunnelling between the two vacua doesn't happen everywhere at the same time, but we have the formation of bubbles which expand, eventually collide and in the end the whole space will be in the true vacuum. Once one computes the decay rate for a specific model, one can obtain the *nucleation temperature* T_n at which one bubble is nucleated per horizon in average.
In particular, the goal of this Chapter is to compute the nucleation temperature in two different scenarios:one is an extension of the Standard Model with a $|H|^6$ operator and the other one involves the existence of a strongly coupled sector that

gives rise to a light dilaton.

3.2 Bubble Nucleation

3.2.1 False Vacuum Decay

In this section we will build the basic toolkit to study bubble nucleation in first order phase transitions [55].
In 1977 S. Coleman and C. Callan derived the decay rate of the false vacuum [75, 76], later in 1980, A. Linde included finite temperature effects in the computation [77, 78]. Using these results, the tunneling rate per unit volume is given by:

$$\Gamma(T) \simeq \max\left[T^4\left(\frac{S_3/T}{2\pi}\right)^{3/2}\exp\left(-S_3/T\right), R_0^{-4}\left(\frac{S_4}{2\pi}\right)^2\exp\left(-S_4\right)\right] \tag{3.1}$$

where R_0 is the bubble radius at nucleation, while S_3 and S_4 are, respectively, the 3-dimensional and the 4-dimensional Euclidean action of the $O(3)$- and $O(4)$-symmetric tunnelling solutions, which are given by:

$$S_3 = 4\pi\int dr\, r^2\left[\frac{1}{2}\phi'(r)^2 + V(\phi(r))\right] \tag{3.2}$$

$$S_4 = 2\pi^2\int dr\, r^3\left[\frac{1}{2}\phi'(r)^2 + V(\phi(r))\right] \tag{3.3}$$

where $V(\phi)$ is the potential and $\phi(r)$ is the field configuration which interpolates between the two asymptotic vacuum.

The $O(3)$ bounces are described by the coordinate $r = \vec{x}$ and have $d = 3$ dimensions, while the $O(4)$ bounces are described by the coordinate $r = \sqrt{\vec{x}^2 + t^2}$ and have $d = 4$ dimensions. Moreover, the former are induced by thermal effects, while the latter are quantum-induced.

From the extremization of the action we obtain the Euclidean equation of motion:

$$\phi''(r) + \frac{d-1}{r}\phi'(r) = \frac{dV}{d\phi} \tag{3.4}$$

with boundary conditions:

$$\phi'(0) = 0 \qquad \lim_{r\to\infty}\phi(r) = 0 \tag{3.5}$$

It is useful to interpret this problem as the study of the evolution of a particle moving in a potential $-V(\phi(r))$ with a friction term $\frac{d-1}{r}\frac{d\phi}{dr}$, where r parameterize the time and ϕ is the position of the particle. The particle starts with zero velocity

and at $r \to \infty$ stops at $\phi = 0$.
It has been proved [75] that there is always a solution to equations (3.4) and (3.5) by means of an undershoot/overshoot argument. If the initial position of the particle is too close to the true vacuum, it will have enough energy to move over the false vacuum with non-zero velocity: we have an overshoot configuration and the solution will be divergent. Conversely, if the initial position of the particle is too close to the false vacuum, the particle will not have enough energy to reach the true vacuum because of the friction term: we have an undershoot configuration and the solution will be oscillatory. Therefore, by continuity there will be an intermediate initial position for which the particle rests in the false vacuum and for which we have our bounce solution.

Analytical solutions of the bounce action: the thick-wall limit

Besides the numerical procedure inspired by the overshoot/undershoot argument, one can estimate the bounce actions by semi-analytical or analytical expressions. For the latter, in particular, there are two classes of potentials that give an analytical estimate for the bounce action: the *thin-wall* limit and the *thick-wall* limit [55].

In the thin-wall limit the extrema of the potential are nearly degenerate and they are separated by a large barrier, while for the thick-wall limit the potential barrier is small when compared to the potential energy difference.
As anticipated, we will compute the nucleation temperature in the thick-wall limit, which is known to be a good approximation for the potentials that we are going to consider. Let us consider the $O(3)$-symmetric vacuum bubbles [79, 80]. The potential V has a false vacuum: let's say that $\phi_{FV} = 0$ and $V(\phi_{FV}) = 0$. The true minimum is at $\phi = \phi_0$. Now let's consider a bubble of the true vacuum and radius R inside an exterior of false vacuum. Outside the bubble, the potential is zero and the ϕ-profile is constant, therefore only the region inside the bubble will contribute to the action. If $\phi_* = \phi(0)$ is the initial field value, at which the bounce starts, $\delta\phi = \phi_*$ is the total variation of ϕ inside the bubble wall δR, where the bubble wall is defined as the region r where ϕ varies. Starting from Eq. (3.2), the action can be approximated as:

$$S_3 \simeq 2\pi R^2 \left(\frac{\delta\phi}{\delta R}\right)^2 \delta R + \frac{4}{3}\pi R^3 \bar{V} \tag{3.6}$$

where $\bar{V} < 0$ is the potential energy averaged in the bubble wall. We will take the approximation $\bar{V} = V(\phi_*) - V(0) = V(\phi_*)$. If the bubble is thick, one can take $\delta R = R$. We define the *critical radius* R_c of the bubble by extremizing Eq. (3.6)

with respect to R:

$$\frac{\delta S_3}{\delta R} = 0 \rightarrow R_c^2 = \frac{\phi_*^2}{-2V(\phi_*)} \tag{3.7}$$

Then we obtain the action by injecting the critical radius (3.7) in Eq. (3.6). The result is:

$$S_3 = \frac{4\pi}{3} \frac{\phi_*^3}{\sqrt{-2V(\phi_*)}} \tag{3.8}$$

Similarly, for the $O(4)-$ bounce solutions, one can obtain the formulas:

$$S_4 = \frac{\pi^2}{2} \frac{\phi_*^4}{-V(\phi_*)}, \qquad R_c^2 = \frac{\phi_*^2}{-V(\phi_*)} \tag{3.9}$$

3.3 Gravitational Waves from First Order Phase Transitions: Thermodynamical Parameters

First Order Phase Transitions can produce GWs in different ways and our understanding on the generation of the signal relies on hydrodynamic simulations (for more details, see e.g. the review [81]). We can identify three possible contributions and stages to the GW signal $\Omega_{GW} \equiv \rho_{GW}/\rho_{crit}$, where $\rho_{crit} = 3H^2/(8\pi G)$ is the critical density:

1. **Bubble collision contribution** Ω_{bc} bubbles of true vacuum collide and merge.

2. **Sound waves contribution** Ω_{sw} after bubble have collided and merged, the shells of fluid kinetic energy propagate int he plasma as sound waves, which eventually overlap.

3. **Magnetohydrodynamic turbulence** Ω_{tu} as the sound waves propagate, non-linearities in the plasma become important and the fluid shells eventually develop shocks.

The total power spectrum can be approximated as the sum of the three contributions above:

$$\Omega_{GW} = \Omega_{bc} + \Omega_{sw} + \Omega_{tu} \tag{3.10}$$

The key parameters that enter in the prediction of the GW spectrum are four: the nucleation temperature T_n, the phase transition strength α, the phase transition rate β and the bubble wall speed v_w. These quantities can be computed from the Lagrangian of the theory, hence the measurement of GW spectrum becomes another probe of new physics.
In the following, we proceed to define the GW parameters that we have mentioned above.

Nucleation Temperature The temperature at which the two minima are degenerate is called *critical temperature* T_c and below this temperature the decay of the false vacuum becomes energetically possible.
The *nucleation temperature* T_n is defined as the temperature at which one bubble is nucleated per horizon on average

$$N(T_n) = \int_{T_n}^{T_c} \frac{dT}{T} \frac{\Gamma(T)}{H(T)^4} = 1 \tag{3.11}$$

which implies:

$$\Gamma(T_n) \simeq H(T_n)^4 \tag{3.12}$$

The decay rate $\Gamma(T)$ is computed in the specific model, whereas the Hubble rate is given by:

$$H(T)^2 = \frac{1}{3M_{pl}^2}(\rho_{rad} + \rho_{vac} + \rho_{wall}) \tag{3.13}$$

with $M_{Pl} = 1/\sqrt{8\pi G_N} = 2.43 \cdot 10^{18}$ GeV and

$$\rho_{wall} \approx 0 \qquad \rho_{rad} = \frac{\pi^2 g_*}{30} T^4 \qquad \rho_{vac} = \Delta V \tag{3.14}$$

where g_* is the number of effective relativistic degrees of freedom in the radiation bath, for example $g_*^{\rm SM} = 106.75$ is the value for SM particles at temperatures higher than the top quark mass and ΔV is the difference between the potential in the two minima. In Eq. (3.13) we did not include the contribution from the non-relativistic particles since their energy density is exponentially smaller than the one of relativistic species, i.e. $\rho_{matter} \propto \exp\left[-(m-\mu)/T\right]$.

Phase Transition Strength The strength of the phase transition is given by the parameter α, which is defined as the the latent heat of the transition divided by the radiation energy of the Universe:

$$\alpha = \frac{\Delta V - \frac{T/4}{\frac{\partial \Delta V}{\partial T}}}{\rho_{rad}} \simeq \frac{\Delta V}{\rho_{rad}} \tag{3.15}$$

which is evaluated at the nucleation temperature. It parameterizes the amount of energy available for the production of Gravitational Waves.

Phase Transition Duration Another important parameter is the transition rate parameter of the phase transition β_H, which can be thought as the inverse phase transition duration. It can be defined from the bubble nucleation rate as follows:

$$\beta = -\frac{dS_d}{dt}\bigg|_{T_{nuc}} \simeq \frac{\dot{\Gamma}}{\Gamma} \Longrightarrow \beta_H \equiv \frac{\beta}{H_n} = T\frac{dS_d}{dT}\bigg|_{T_{nuc}} \tag{3.16}$$

where $H_n \equiv H(T_{nuc})$ and $d = 3, 4$, depending on whether the bubble nucleation happens via $O(3)$ or $O(4)$ tunnelling.

Wall velocity The last parameter is the so-called wall velocity v_w, which chareterizes the speed at which the bubble is expanding. In order for the bubble to expand, the pressure inside must be larger than the exterior one and this happens when $\Delta V < 0$. In other words, the vacuum energy difference between the broken and the symmetric phase accelerates the bubble wall. Entering the broken phase, particles which are coupled to the scalar field driving the phase transition acquire a mass, which is proportional to the VEV. Then, the scalar field gradient along the wall profile induces a retarding friction pressure, due to the interaction with the particles in the plasma. The terminal velocity of the bubble wall will depend on the equilibrium between this pressure and the accelerating vacuum pressure [55]. Determining the wall velocity is a non-trivial problem, since it requires an accurate study of the plasma around the bubble wall. In the literature, different methods and regimes have been considered. For a pedagogical introduction to the problem we refer the reader to [55], while for the current state of the art we refer the reader to Ref. [82].

3.4 Supercool phase transitions

When the vacuum energy dominates the energy density of the Universe, the phase transition is said to be *supercool*, i.e.:

$$\alpha \gg 1 \qquad \text{supercooling} \tag{3.17}$$

Supercool phase transitions are expected when we have potentials which are flat enough at the origin at zero temperature. These potentials are obtained in theories with an approximate scale invariance: the Coleman-Weinberg potential in the weakly-coupled scenario and the light-dilaton potential in the strongly-coupled scenario. We'll discuss in more detail the latter one in Sec. 3.6.

Nearly-conformal potentials lead to interesting cosmological consequences because of the temperature dependence of the tunneling action, which is very different from other potentials that give a first order phase transition [83]. The nucleation temperature is determined by the tunnelling point since $T_n \propto \phi_R$, where we define ϕ_R as the release point of our bounce solution. Nearly-conformal potentials have a maximum at ϕ_{max} and a minimum at ϕ_{min} which are widely separated and we have $\phi_R \gtrsim \sqrt{\phi_{max}\phi_{min}} \ll \phi_{min}$. Therefore we can have very small T_n compared to the vacuum expectation value ϕ_{min}. However the critical temperature is $T_c \propto \phi_{min}$. Therefore the nucleation temperature is much smaller than the critical temperature, and in the regime between the two temperatures, the vacuum

energy dominates, leading to an additional period of inflation. The amount of supercooling is estimated by the number of efolds N_e during inflation:

$$N_e \sim \log \frac{T_c}{T_n} \tag{3.18}$$

Possible cosmological consequences of supercooling are, for example, a large gravitational wave spectrum [84], a dilution of any pre-existing relic (such as dark matter, baryon or other asymmetries, topological defects and gravitational waves [85, 86, 87]) or effects on the bubble wall velocity[55].

3.5 $|H|^6$ Effective Field Theory

3.5.1 The Effective Potential and its high temperature limit

Let us add in the classical Higgs potential a dimension-six $|H|^6$ operator:

$$V(H) = m^2 |H|^2 + \lambda |H|^4 + \frac{|H|^6}{\Lambda^2} \tag{3.19}$$

where $H^T = (\chi_1 + i\chi_2, \varphi + i\chi_3)/\sqrt{2}$ and Λ is the scale of validity of the model, that is the energy below which we expect that our Effective Field Theory breaks down due to the loss of unitarity. Furthermore, one of the first studies [88] on this class of potential analyzes the constraints on Λ in order to have a successful first order phase transition. The constraints on Λ depend on the physical mass m_h of the Higgs boson: we have a lower bound on Λ to ensure the existence of the true minimum at $T = 0$ and an upper bound on Λ to make sure that the phase transition is of the first order. For $m_h = 125\,\text{GeV}$, we have $484\,\text{GeV} \lesssim \Lambda \lesssim 840\,\text{GeV}$. By expanding the Higgs around its vacuum expectation value (VEV) $\varphi = \phi + h$ one obtains:

$$V_{tree}(\phi) = \frac{m^2}{2}\phi^2 + \frac{\lambda}{4}\phi^4 + \frac{1}{8}\frac{\phi^6}{\Lambda^2} \tag{3.20}$$

with

$$m^2 = -\frac{m_h^2}{2} + \frac{3}{4}\frac{v^4}{\Lambda^2}, \tag{3.21}$$

$$\lambda = \frac{1}{2}\frac{m_h^2}{v^2} - \frac{3}{2}\frac{v^2}{\Lambda^2} \tag{3.22}$$

where $v = 246\,\text{GeV}$ is the VEV of the Higgs field.

On top of the tree level result we need to compute the one-loop corrections. In the Early Universe, we can't neglect the interaction with matter and radiation and we are required to use Thermal Field Theory. The one-loop corrections are

computed as the sum of all the 1PI diagrams with a single loop and zero external momenta. In the computation we have to use the Feynman rules derived in Thermal Field theory (see the review [89] for further details). In the radiative corrections we need to consider the contributions of the gauge and Higgs bosons and of the top quark, whereas the other contributions from the other SM fermions are negligible. The one-loop corrections at finite temperature in the Landau gauge (where ghosts decouple) are:

$$\Delta V_1(\phi, T) = \sum_{i=\{h,\chi,W,Z,t\}} \frac{n_i T}{2} \sum_{n=-\infty}^{+\infty} \int \frac{d^3\vec{k}}{(2\pi)^3} \log[\vec{k}^2 + \omega_n^2 + m_i^2(\phi)] \tag{3.23}$$

where $k_E(\omega_n, \vec{k})$ is the Euclidean loop 4-momentum, ω_n are the Matsubara frequencies in the imaginary time formalism, where $\omega_n = 2n\pi T$ for bosons and $\omega_n = 2(n+1)\pi T$ for fermions. The number of degrees of freedom are $n = \{1, 3, 6, 3, -12\}$. The masses $m_i^2(\phi)$ in Eq. (3.23) read:

$$m_h^2(\phi) = m^2 + 3\lambda\phi^2 + \frac{15}{4}\frac{\phi^4}{\Lambda^2} \tag{3.24}$$

$$m_\chi^2(\phi) = m^2 + \lambda\phi^2 + \frac{3}{4}\frac{\phi^4}{\Lambda^2} \tag{3.25}$$

$$m_W^2(\phi) = \frac{g_2^2}{4}\phi^2 \tag{3.26}$$

$$m_Z^2(\phi) = \frac{g_1^2 + g_2^2}{4}\phi^2 \tag{3.27}$$

$$m_t^2(\phi) = \frac{y_t^2}{2}\phi^2 \tag{3.28}$$

The one-loop corrections can be decomposed in a temperature independent term and temperature dependent term. The former piece coincides with $T = 0$ one-loop corrections in Quantum Field Theory, which were first derived by S. Coleman and E. Weinberg in 1973 [90]. Upon regularizing the theory with a cut-off and imposing, via the on-shell renormalization scheme, that the minimum of the potential corresponds to the Higgs VEV v and that the second derivative of the potential corresponds to the Higgs mass, in the end the $T = 0$ one-loop contributions to the tree level potential are given by:

$$\Delta V_1^0(\phi) = \sum_{i=\{h,W,Z,t\}} \frac{n_i}{64\pi^2}\left[m_i^4(\phi)\left(\log\frac{m_i^2(\phi)}{m_i^2(v)}\right) + 2m_i^2(v)m_i^2(\phi)\right] \tag{3.29}$$

For the Goldstone bosons, we can't use Eq. (3.29) since in the true vacuum their masses are equal zero, i.e. $m_\chi(\phi = v) = 0$, and the potential becomes IR divergent. In [91] it was pointed out that for the Higgs boson it would be better to define renormalization conditions which take into account the running of self-energy from $p^2 = 0$ (where the effective potential is defined) to $p^2 = m_h^2$ (where the physical Higgs mass is defined). At the end of the renormalization procedure, one obtains that the Goldstone contribution to the zero-temperature effective potential is:

$$\Delta V_1^{0,(\chi)}(\phi) = \frac{n_\chi}{64\pi^2} m_\chi^2(\phi)\left(\log\frac{m_\chi^2(\phi)}{m_h^2} - \frac{3}{2}\right) \tag{3.30}$$

The finite temperature corrections, which were first computed by L. Dolan and R. Jackiw [92] in 1973, are given by:

$$\Delta V_1^T(\phi, T) = \sum_{i=h,\chi,W,Z,t} \frac{n_i T^4}{2\pi^2}\int_0^\infty dk k^2 \log\left[1 \mp \exp -\sqrt{k^2 + m_i^2(\phi)/T^2}\right] \tag{3.31}$$

$$\equiv \sum_{i=\text{bosons}} \frac{n_i T^4}{2\pi^2} J_b\left(\frac{m_i^2(\phi)}{T^2}\right) + \sum_{i=\text{fermions}} \frac{n_i T^4}{2\pi^2} J_f\left(\frac{m_i^2(\phi)}{T^2}\right) \tag{3.32}$$

where the minus (plus) sign stands for bosons (fermions). The functions $J_{b/f}$, by Taylor-expanding in the high temperature limit ($x \equiv \frac{m_i(\phi)}{T} \to 0$), take the form:

$$J_b(x) = -\frac{\pi^4}{45} + \frac{\pi^2}{12}x - \frac{\pi}{6}x^{3/2} - \frac{x^2}{32}\log\frac{x}{a_b} + \mathcal{O}\left(x^3 \log\frac{x^{3/2}}{const.}\right) \tag{3.33}$$

$$J_f(x) = \frac{7\pi^4}{360} - \frac{\pi^2}{24}x - \frac{x^2}{32}\log\frac{x}{a_f} + \mathcal{O}\left(x^3 \log\frac{x^{3/2}}{const.}\right) \tag{3.34}$$

with $\log a_b \simeq 5.4076$ and $\log a_f \simeq 2.6350$.
This one-loop result can't still be truthfully considered complete, due to the presence of higher loop corrections of the same order and whose leading contribution is given by the so called *daisy diagrams*. They are N ring diagrams, where $N-1$ loops are attached to a main one. The daisy diagrams only need to be resummed in the IR-limit of vanishing momenta running in the petals. One can prove that resumming the daisy diagrams amounts to shift the masses of the bosons [93]:

$$m_b^2(\phi) \to m_b^2(\phi) + \Pi_b(T) \tag{3.35}$$

where $\Pi_b(T)$ is the self-energy of the bosonic field b in the IR limit, $\omega = \vec{p} = 0$, also known as the *Debye mass*. These diagrams are needed since we have a breakdown of the perturbative expansion due to IR divergences (i.e. $m \lesssim T$), hence they are relevant at high temperature where the particles can be approximated as nearly

massless. In particular, bosonic fields have a vanishing Matsubara frequency that will behave as a massless degree of freedom and generate IR-divergences at high-temperature, while the other non-zero modes ω_n act as a mass of order T and they are negligible. On the other hand, fermionic fields do not have a massless mode, thus they do not need to be resummed.

Taking into account the above resummation, the daisy corrections to the potential are given by [91]:

$$\Delta V_{daisy} = \sum_{i=\{h,\chi,W,Z\}} \frac{\bar{n}_i T}{12\pi}\left[m_i^3(\phi) - \left(m_i^2(\phi) + \Pi_i(T)\right)^{3/2}\right] \tag{3.36}$$

where $\bar{n} = \{1, 3, 2, 1, 1\}$ and $\Pi_i(T)$ are the Debye masses for our relevant bosonic fields. The latter take the form [91]:

$$\Pi_{h,\chi}(T) = \frac{T^2}{4v^2}(m_h^2 + 2m_W^2 + m_Z^2 + 2m_t^2) - \frac{3T^2}{4}\frac{v^2}{\Lambda^2} \tag{3.37}$$

$$\Pi_W(T) = \frac{22}{3}\frac{m_W^2}{v^2}T^2 \tag{3.38}$$

$$\Pi_Z(T) = \frac{22}{3}\frac{(m_Z^2 - m_W^2)}{v^2}T^2 - m_W^2(\phi) \tag{3.39}$$

$$\Pi_\gamma(T) = m_W^2(\phi) + \frac{22}{3}\frac{m_W^2}{v^2}T^2 \tag{3.40}$$

By summing the tree level term (3.20), the one-loop corrections (3.29)-(3.30) and the daisy diagrams (3.36), we find the total effective potential in the Landau gauge reads :

$$\begin{aligned} V_{eff}(\phi, T) = &\sum_{i=\{h,W,Z,t\}} \frac{n_i}{64\pi^2}\left[m_i^4(\phi)\left(\log\frac{m_i^2(\phi)}{m_i^2(v)}\right) + 2m_i^2(v)m_i^2(\phi)\right] \\ &+\frac{n_\chi}{64\pi^2}m_\chi^2(\phi)\left(\log\frac{m_\chi^2(\phi)}{m_h^2} - \frac{3}{2}\right) \\ &+ \sum_{i=h,\chi,W,Z,t} \frac{n_i T^4}{2\pi^2}\int_0^\infty dk k^2 \log\left[1 \mp \exp -\sqrt{k^2 + m_i^2(\phi)/T^2}\right] \\ &+ \sum_{i=\{h,\chi,W,Z\}} \frac{\bar{n}_i T}{12\pi}\left[m_i^3(\phi) - \left(m_i^2(\phi) + \Pi_i(T)\right)^{3/2}\right] \end{aligned} \tag{3.41}$$

However, to simplify the numerical computation, we'll use the high-temperature expansion of the effective potential:

$$V_{eff}(\phi, T) \overset{T\gg v}{\simeq} D(T^2 - T_0^2)\phi^2 - ET\phi^3 + \frac{\lambda(T)}{4}\phi^4 + \frac{1}{8}\frac{\phi^6}{\Lambda^2} \tag{3.42}$$

with:

$$D = \frac{2\lambda v^2 + 2m_W^2 + m_Z^2 + 2m_t^2}{8v^2} \tag{3.43}$$

$$E = \frac{2m_W^3 + m_Z^3}{4\pi v^3} \tag{3.44}$$

$$T_0^2 = \frac{m_h^2 - 3/2v^4/\Lambda^2 - 8Bv^2}{4D} \tag{3.45}$$

$$B = \frac{3}{64\pi^2 v^4}(2m_W^4 + m_Z^4 - 4m_t^4) \tag{3.46}$$

$$\lambda(T) = \lambda + \left(\frac{T}{\Lambda}\right)^2 - \frac{3}{16\pi^2 v^4}\left(2m_W^4 \log\frac{m_W^2}{A_B T^2} + 2m_Z^4 \log\frac{m_Z^2}{A_B T^2} - 4m_t^4 \log\frac{m_t^2}{A_F T^2}\right) \tag{3.47}$$

where $\log A_B = \log a_b - 3/2$ and $\log A_F = \log a_b - 3/2$. The Eqs. (3.42)-(3.47) are obtained by substituting Eqs. (3.34)-(3.33) in the finite temperature corrections Eq. (3.31).

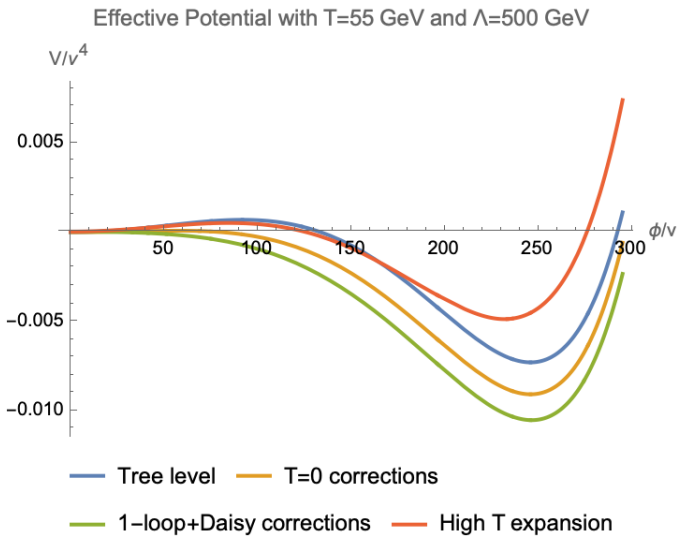

Figure 3.1: Effective Potential in the Landau gauge for the extension of the Standard Model with a dimension six $|H|^6$ operator with $T = 55\,GeV$ and $\Lambda = 500\,GeV$. The plot shows: the potential at tree level, the potential with $T = 0$ 1-loop corrections, the potential with the full 1-loop and daisy corrections, the potential in the high temperature limit.

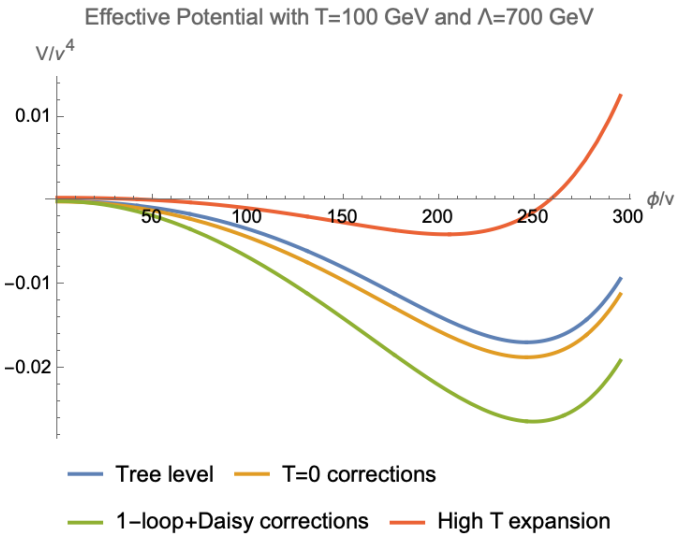

Figure 3.2: Effective Potential in the Landau gauge for the extension of the Standard Model with a dimension six $|H|^6$ operator with $T = 100\,GeV$ and $\Lambda = 700\,GeV$. The plot shows: the potential at tree level, the potential with $T = 0$ 1-loop corrections, the potential with the full 1-loop and daisy corrections, the potential in the high temperature limit.

3.5.2 Numerical Computation and Results

We want to compute the nucleation temperature in the case for $O(3)$ tunneling, by employing the bounce action S_3 in the thick-wall limit. We will compute the initial field value ϕ_* using the bounce solution obtained via the undershoot/overshoot algorithm.
The first step is the solution of the differential equation (3.4) with boundary conditions (3.5), whose numerical solution is not straightforward. However we can turn this boundary value problem into an equivalent Cauchy problem, with initial conditions:

$$\phi(x_{min}) = a \tag{3.48}$$

$$\phi'(x_{min}) = 0 \tag{3.49}$$

where a is the initial value of the field, which we will determine via the shooting method and thus it is usually called *shooting parameter*. This shooting parameter is the ϕ_* that we have previously introduced. Moreover, we notice that we have defined our initial conditions in x_{min}, since in $x = 0$ we have a singularity. Once we have the solution of Eq. (3.4) as a function of the parameter a, we will find the value of the shooting parameter by requiring that the solution will go to zero

at $x \to \infty$, which is the other boundary condition of our problem. However,in practice, we will require this condition to be satisfied at a value x_{max}, namely:

$$\phi(x_{max}) = 0 \tag{3.50}$$

The computation boils down to a root finding problem, which we choose to solve via the bisection method. In order to start implementing the algorithm, we have to decide the interval in which we look for the solution. We choose two values of the parameter, the lower bound is given by the value of the shooting parameter for which we expect the solution to undershoot (`under`) and while the upper bound gives an overshoot solution (`over`): we know that the solution will lie between these two values because of our discussion in Section 3.2.1. Choosing the initial interval is actually quite even more tricky due to the dependence on Λ and T in our potential and, ultimately, in the existence of the bounce solution. Therefore we decide to pick an arbitrary small positive real number as `under`, for which we check that the solution undershoots, and a value of `over`, where the initial position is given by the value of the field at the true minimum of the potential for temperatures around slightly above T_0 to allow the existence of a bounce solution.

Once we have found our bounce solution, we can compute the corresponding action in the thick-wall limit using Eq. (3.8) and we evaluate the decay rate and the Hubble rate using respectively the formulas (3.1) and (3.13). The last step is to build a numerical function, `Tnucl[`Λ`]` using the condition (3.12). We have to look for the root of this function using again the standard bisection method. The temperature range where we search for the solution is between $\mathcal{O}(10)$ GeV and the critical temperature. The result is showed in Figure 4.3.

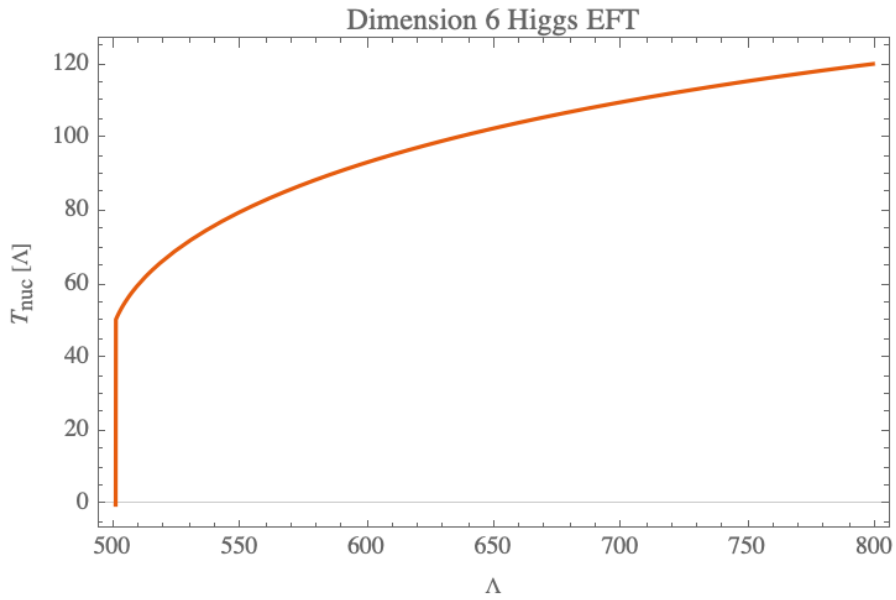

Figure 3.3: Nucleation temperature for $O(3)$-symmetrical bounce using the thick wall formula

We observe that we were able to reproduce the growing profile and order of magnitude of the nucleation temperature, but we struggled to match perfectly the temperatures for lower values of the cutoff from other known studies in literature (see for example [94], where the bounce action is computed numerically). This result could be due to both our numerical procedure and our approximation for the potential.

To summarise, we find that the transition is indeed of the first order, but it can't be supercooled, since $T_{nuc} \ll v$, for the values of Λ for which the Effective Field Theory is well defined. In the next section we will discuss anoter new physics scenario, which gives rise to a supercool phase transition.

3.6 The light-dilaton potential

3.6.1 The dilaton potential

The dilaton potential at $T = 0$

Let us consider a strongly-coupled sector in the UV where an approximate scale symmetry holds [95, 96]. When this symmetry gets spontaneously broken, we will have in the spectrum a pseudo-Nambu Goldstone boson (pNGB), which is called

the *dilaton*. If the dilaton is the lightest state of this nearly-conformal sector, we can integrate out all the other dynamical fields: the phase transition can be described in terms of the dilaton VEV only.
Since it is not possible to break the conformal symmetry in a purely spontaneous way, we break it explicitly by adding the strong sector operator:

$$\epsilon \mathcal{O}_\epsilon \tag{3.51}$$

with scaling dimension $d = 4 + \gamma_\epsilon \lesssim 4$ (for the anomalous dimension one has $\gamma_\epsilon \geq -3$ because of the unitarity bound on scalar CFT operator [95]). Provided $|\gamma_\epsilon| \ll 1$ and ϵ at the UV scale is somewhat small too, ϵ only slowly grows when running towards the IR. The nearly-conformal invariance is then maintained for a large energy range. However, at some small energy, the contribution of O_ϵ becomes so large that the strong sector condensates and scale invariance is broken, thus generating the confinement scale f and the dilaton.
The dilaton is defined by its transformation rule

$$\chi(x) \longrightarrow \lambda \chi(x/\lambda) \tag{3.52}$$

under dilatations $x_\mu \to x_\mu/\lambda$. We can parameterise the dilaton as follows [97] :

$$\chi(x) = f e^{\frac{\sigma(x)}{f}} \tag{3.53}$$

where $\sigma(x)$ transforms non-linearly under dilatations $\sigma(x) \longrightarrow \sigma(\lambda x) + f \log \lambda$.
Now let us write down the potential for the model. Because of scale invariance we can write down a χ^4 term, which is either unbounded from below or it yields a vanishing VEV, with no pNGB in the spectrum. The slightly relevant operator generates another term in the potential $\epsilon(\chi)\chi^4$. Therefore the dilaton potential at $T = 0$ reads:

$$V_\chi^{T=0}(\chi) = c_\chi g_\chi^2 \chi^4 - \epsilon(\chi)\chi^4 \tag{3.54}$$

where c_χ is $\mathcal{O}(1)$ constant and $g_\chi \gtrsim 1$ is a typical coupling constant of the strong sector. Now, the running of the coupling ϵ, with μ as the renormalization scale,

$$\frac{\partial \epsilon}{\partial \log \mu} \simeq \gamma_\epsilon \epsilon \tag{3.55}$$

leads to a non-zero VEV f for the dilaton:

$$\left.\frac{dV}{d\chi}\right|_{\chi=f} = 0 \quad \to \quad \epsilon(\chi) = \frac{c_\chi g_\chi^2}{1 + \gamma_\epsilon/4} \left(\frac{\chi}{f}\right)^{\gamma_\epsilon} \tag{3.56}$$

and a mass for the dilaton, whose smallness is linked to the smallness of the anomalous dimension:

$$m_\sigma^2 = \left.\frac{\partial}{\partial \sigma^2} V(\chi(\sigma))\right|_{\sigma=0} \quad \to \quad \gamma_\epsilon \simeq -\frac{1}{c_\chi} \frac{m_\sigma^2}{g_\chi^2 f^2} \tag{3.57}$$

Finally, we can write the dilaton potential as:

$$V_\chi^{T=0}(\chi) = c_\chi g_\chi^2 \chi^4 \left(1 - \frac{1}{1+\gamma_\epsilon/4}\left(\frac{\chi}{f}\right)^{\gamma_\epsilon}\right) \tag{3.58}$$

From equation (3.57) we notice that the conformal limit $|\gamma_\epsilon| \ll 1$ coincides with the light dilaton limit $y_\chi \equiv \frac{m_\sigma}{f} \ll 1$.
Finally, the vacuum energy in the unbroken phase is given by:

$$\Delta V = V(\chi = 0) - V(\chi = f) \simeq \left(\frac{m_\sigma f}{4}\right)^2 \tag{3.59}$$

Here we have assumed that the Higgs VEV is smaller than the one of the dilaton, thus neglecting its contribution to the vacuum energy.

An holographic perspective The 4D strongly coupled theory that we have described above can be mapped into a 5D weakly-coupled theory with AdS_5 metric via the AdS-CFT correspondence [98]. The dual 5D theory predicts non-canonical kinetic terms:

$$\mathcal{L}_K = \frac{Z^2}{2}\partial_\mu\chi\partial^\mu\chi \tag{3.60}$$

We can introduce a canonically normalised compensator field $\chi' \equiv Z\chi$ and $\sigma' \equiv \chi - Zf$ to obtain canonical kinetic terms. This rescaling will lead to the potential:

$$V_{\chi'}^{T=0}(\chi') = \frac{c_\chi}{Z^4} g_\chi^2 \chi'^4 \left(1 - \frac{1}{1+\gamma_\epsilon/4}\left(\frac{\chi'}{Zf}\right)^{\gamma_\epsilon}\right) \tag{3.61}$$

However, in this thesis, we will study only the $Z = 1$ case.
Now let us consider a theory with a warped extra dimension [99] as the 5D dual of our 4D conformal field theory. Using holography arguments to relate the two theories, one can derive that the coupling constant of the strong sector is [65, 100]:

$$g_\chi = \frac{4\pi}{N} \tag{3.62}$$

This relation is true for a glueball-like dilaton [101].

The dilaton potential at finite temperature

In the usual 4D QFT perspective, we can compute the thermal corrections to the potential, which are generated by the particles in the plasma.
When the temperature is well below $g_\chi f$, the confined phase is the thermodynamically most favorable phase, whereas in the opposite temperature regime the

deconfined phase is the most favorable one. For $\chi = 0$, the strong sector is in its deconfined phase. By dimensional analysis and large N-counting the free energy in this phase scales as:

$$F_{\rm CFT}(\chi = 0) \simeq -bN^2T^4 \tag{3.63}$$

The constant b depends on the number of degrees of freedom per color in the strong sector. For definiteness, we will consider $\mathcal{N} = 4$ $SU(N)$ super Yang-Mills (SYM). Then the result is [102]:

$$b = \frac{\pi^2}{8} \tag{3.64}$$

It is reasonable to expect that any realistic strong sector has a similar number of degrees of freedom as $\mathcal{N} = 4$ $SU(N)$ SYM and that the free energy is not much different from the one we use. Moreover, we are neglecting the degrees of freedom of the SM particles and of the techni-quarks of the strong sector, thus keeping only the contribution of the techni-gluons.
When $\chi \gtrsim T/g_\chi$ the finite temperature corrections are given by the SM thermal corrections, that can be neglected. In the regime $0 \lesssim \chi \lesssim T/g_\chi$, without a precise UV description, the exact form of the free energy is not known since the theory is in the strongly coupled regime. However, in our description we can assume [84, 95] that the dilaton still approximately exists and we add the thermal corrections from N^2 CFT degrees of freedom to its zero temperature potential. The thermal corrections of the dilaton potential read:

$$\Delta V_T^{1-\rm loop}(\chi, T) = \sum_{\rm CFT\,bosons} \frac{nT^4}{2\pi^2} J_b\left(\frac{m_{CFT}^2}{T^2}\right) \tag{3.65}$$

where n is the degeneracy factor of each bosonic state, with mass $m_{CFT} = g_\chi \chi$, and J_b is defined as in Eq. (3.31). Then we choose the normalization:

$$\sum_{\rm CFT\,bosons} n = \frac{45N^2}{4} \tag{3.66}$$

in order to recover the free energy in the deconfined phase at $\chi = 0$.

In the end, the finite-temperature effective potential for the dilaton is:

$$V(\chi, T) = V_\chi^{T=0}(\chi) + \Delta V_T^{1-\rm loop}(\chi, T) \tag{3.67}$$

where $V_\chi^{T=0}(\chi)$ and $\Delta V_T^{1-\rm loop}(\chi, T)$ are defined respectively in Eq.(3.58) and Eq.(3.65).

3.6.2 Bounce action in the thick wall limit and nucleation temperature

We will compute the nucleation temperature by employing the thick-wall formula for the $O(4)$-bounce [55, 96]. First, we write the effective potential (3.67) in the

following way:

$$V(\chi) - V(0) \simeq \begin{cases} \frac{m_{eff}^2}{2}\chi^2 - \lambda_{eff}(\chi)\chi^4 & \text{if } \chi \lesssim T/g_\chi \\ \\ bN^2T^4 - \lambda_{eff}(\chi)\chi^4 & \text{if } \chi \gtrsim T/g_\chi \end{cases} \tag{3.68}$$

with:

$$m_{eff}^2 \equiv \frac{15}{16}N^2 g_\chi^2 T^2 \tag{3.69}$$

$$\lambda_{eff} \equiv c_\chi g_\chi^2 \left[1 - \frac{1}{1+\gamma_\epsilon/4}\left(\frac{\chi}{f}\right)^{\gamma_\epsilon}\right] \simeq |\gamma_\epsilon| c_\chi g_\chi^2 \log\frac{f}{\chi} \tag{3.70}$$

where we have expanded λ_{eff} in the conformal limit $\gamma_\epsilon \to 0$. The first line of Eq. (4.34) is obtained by expanding $J_b(m_{CFT}^2/T^2)$ in Eq. (3.65) in the high temperature limit using Eq. (3.33), while the second line is obtained by considering the low-temperature limit $J_b(x) \underset{x\to\infty}{\sim} 0$. We plug Eq. (4.34) into Eq. (3.9), obtaining the following expression for the $O(4)$-bounce action:

$$S_4 \simeq \begin{cases} c_* \frac{\pi^2}{2} \underset{\chi_*}{\text{Min}} \frac{\chi_*^4}{-(m_{eff}^2\chi_*^2/2 - \lambda_{eff}\chi_*^4)} & \text{if } \chi_* \lesssim T/g_\chi \\ \\ c_* \frac{\pi^2}{2} \underset{\chi_*}{\text{Min}} \frac{\chi_*^4}{-(bN^2T^4 - \lambda_{eff}\chi_*^4)} & \text{if } \chi_* \gtrsim T/g_\chi \end{cases} \tag{3.71}$$

Here c_* is a coefficient which we fit on the numerical solution. We set:

$$c_* \simeq 2 \tag{3.72}$$

We minimize the expression (3.71) with respect to χ_*. For $\chi_* \gtrsim T/g_\chi$, we obtain $\chi_* = 0$, which is not a viable bounce solution. On the other hand, for $\chi_* \lesssim T/g_\chi$, the minimization of the action yields:

$$S_4 = c_* \frac{\pi^2}{2}\frac{1}{\lambda_*} \tag{3.73}$$

where:

$$\chi_* = \frac{T}{T_c} f \tag{3.74}$$

$$\lambda_* \equiv \lambda_{eff}(\chi_*) = |\gamma_\epsilon| c_\chi g_\chi^2 \log\frac{f}{\chi_*} \tag{3.75}$$

and T_c is the critical temperature, at which the two minima of the free energy are equal:

$$bN^2T_c^4 = \frac{m_\sigma^2 f^2}{16} \implies T_c = \left(\frac{m_\sigma^2 f^2}{16bN^2}\right)^{1/4} = \left(\frac{|\gamma_\epsilon| c_\chi g_\chi^2}{4bN^2}\right)^{1/4} f \tag{3.76}$$

Using the condition (3.12), we find that the nucleation temperature is a solution of:

$$S_4(T_{nucl}) \simeq 4 \ln \frac{R_0^{-1}}{H(T_{nucl})} + \frac{1}{2} \ln \frac{S_4}{2\pi} \tag{3.77}$$

where R_0 is the bubble radius from the thick-wall approximation. Using Eq.(3.9) we obtain:

$$R_0 = \left(\frac{f/m_\sigma}{\sqrt{b} N \log \frac{T_c}{T}} \right)^{1/2} T^{-1} \sim T^{-1} \tag{3.78}$$

The Hubble parameter reads:

$$H^2(T) = H_\Lambda^2 + H_{rad}^2 = \frac{m_\sigma^2 f^2/16}{3M_{pl}^2} + \frac{\pi^2 g_* T^4}{90 M_{pl}^2}, \qquad g_* = 106.75 + \frac{45N^2}{4} \tag{3.79}$$

Notice that in the definition of H_{rad} the expression of ΔV is given by Eq. (3.59) and we have added the degrees of freedom of the strong sector Eq. (3.66) to the ones of the SM particles, for temperatures above the electroweak scale.

We can rewrite the bounce action previously obtained in Eq. (3.73) as:

$$S_4 = \frac{A}{\log T_c/T} \tag{3.80}$$

where:

$$A = c_* \frac{\pi^2}{2} \frac{1}{|\gamma_\epsilon| c_\chi g_\chi^2} = c_* 2\pi^2 \frac{f^2}{m_\sigma^2} \tag{3.81}$$

By substituting Eq.(3.80) into Eq. (3.77) and considering $H \approx H_\Lambda$, the nucleation temperature is given by:

$$T_{nuc} = \sqrt{H_\Lambda T_c} \left(\frac{2\pi}{S_4} \right)^{1/16} \exp\left(\frac{1}{2} \sqrt{-A + \left(\ln \frac{T_c}{H_\Lambda} + \frac{1}{8} \ln \frac{S_4}{2\pi} \right)} \right) \tag{3.82}$$

By neglecting the $S_4/2\pi$ terms, we conclude that there is no nucleation temperature when [103]:

$$A \gtrsim \ln \frac{T_c}{H_\Lambda} \tag{3.83}$$

and that the minimal nucleation temperature is:

$$T_{nuc}^{min} \simeq \sqrt{H_\Lambda T_c} \simeq 0.1 \left(\frac{m_\sigma}{f} \right)^{3/4} \left(\frac{f}{M_{pl}} \right)^{1/2} f \tag{3.84}$$

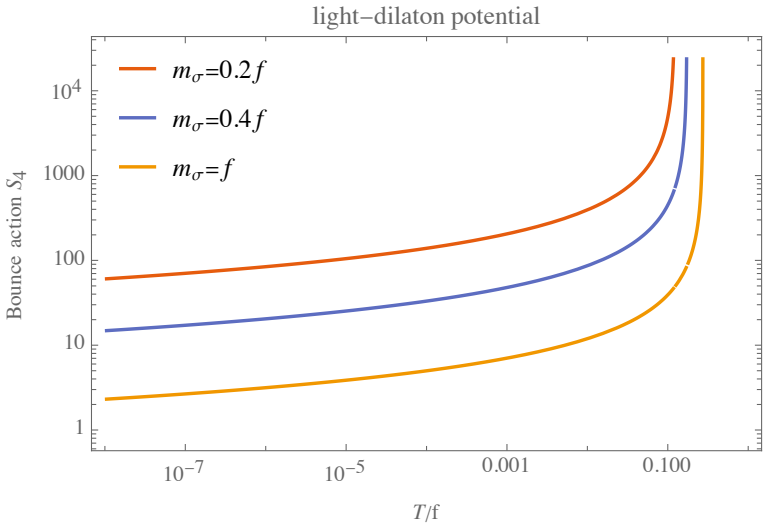

Figure 3.4: $O(4)$ bounce action computed with the thick-wall formula

3.6.3 Numerical Computation and Results

To compute the nucleation temperature we will use the formulas of the previous section. We define:

$$y = \frac{m_\sigma}{f} \tag{3.85}$$

We rewrite all the equations in the previous section in terms of the variable y. Then we can find the root T_{nuc} of Eq. (3.82) by means of a bisection algorithm. Now we have to choose the interval in a different way to take into account the exponential behaviour of our formula for the nucleation temperature. Namely, we choose the minimal nucleation temperature as the minimum of the interval, while the maximum will be 10 times the minimum. However, in order for the bisection method to work, we have to ensure that our function has opposite signs when it is evaluated at the extrema of our interval: when the function is evaluated in the lower extremum, its sign is always negative, whereas the sign in the other extremum has to be checked case by case. Therefore, we increase the maximum by a factor of 10 until the function becomes positive. Moreover we require our algorithm to work only when the square root in Eq.(3.82) is actually positive.
We perform our computation by considering $N = 3$ and using two different values for the confinement scale f.

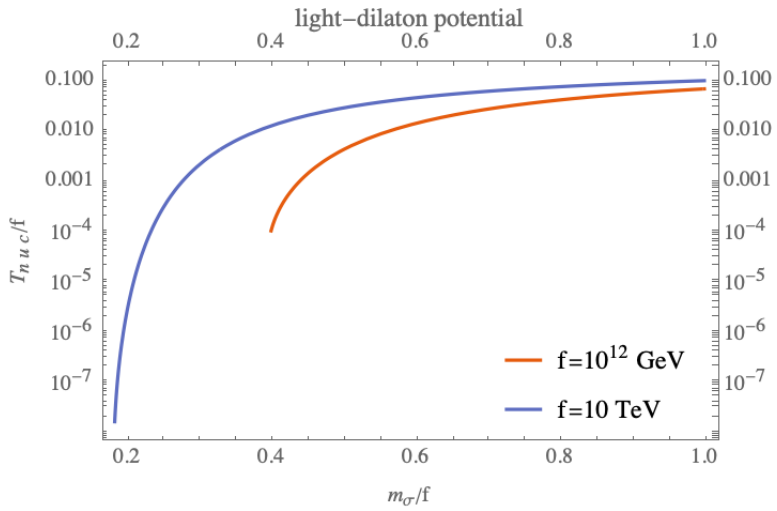

Figure 3.5: Nucleation temperature using the thick-wall formula for $O(4)$ bounce solutions.

We immediately see that the nucleation temperature gets exponentially suppressed as the dilaton mass gets smaller, thus leading to a large amount of supercooling.

3.7 Summary on nucleation temperatures of PTs

In this Chapther we have computed the nucleation temperature for two different extensions of the Standard Model, one with a dimension 6 operator $|H|^6$ and the other with a light dilaton potential, obtained from a strongly coupled sector. In particular, in both cases, we computed the bounce action using the thick-wall formula.
By computing the nucleation temperature, we have actually seen how we can obtain first order phase transitions by extending the Standard Model. We stress that the two different models give rise to different phenomenology, since in the strongly-coupled scenario with the dilaton we have a supercool phase transition. We could have expected that our dimension-6 Effective Field Theory does not lead to a supercool phase transition because the effective potential in the high temperature limit Eq. (3.42) has a polynomial form. In general, polynomial potentials, differently from nearly-conformal potentials, have a maximum and a minimum of the same order and the tunnelling point ϕ_R is of the same order of the value of the field at the minimum of the potential. Therefore, by recalling our discussion in Section 3.4, we can't expect the same hierarchy between the critical temperature and the nucleation temperature, which characterizes supercooling.

On the numerical side, our computation can improved in several ways. Both for the computation of the shooting parameter and for the nucleation temperature, we have adopted the bisection method, however it is known that in the literature there are root finding methods which are more accurate, such as the secant method. Another improvement concerns the stability of our bounce solution in our first computation, which depends on our initial choice of x_{min} and x_{max}, i.e. we don't have control on how our solution varies when we change these initial parameters. Going beyond the thick-wall approximation, it would be interesting to apply the shooting method prescribed in Appendix 6 of [104], where the boundary conditions are improved by a Taylor expansion of the solution.

Chapter 4

Baryogenesis and Gravitational Waves from Dark Matter-Neutron Oscillations

4.1 Introduction

If the signal detected by the PTAs is generated by a First Order Phase Transitions, then the transition must occur below the GeV scale [27]. Therefore, our goal is to look for a mechanism that produces the baryon asymmetry at this scale.
A possible low-scale baryogenesis mechanism was proposed in Ref. [68] by Torsten Bringmann, James Cline and Jonathan Cornell. Their proposal belongs to the class of baryogenesis scenarios that go under the name of *darkogenesis*. These models attempt to link the baryon asymmetry to the existence of dark matter, motivated by the so called *coincidence problem*. The coincidence problem is the observation that the energy density of baryons is only 5 times smaller than the energy density of Dark Matter (DM), i.e. [105]:

$$\frac{\Omega_{\rm CDM}}{\Omega_B} \simeq \frac{0.26}{0.049} \sim 5 \tag{4.1}$$

This coincidence suggests that there might be a mechanisms that generates an asymmetry in both the visible and the dark sector, so DM would also be *asymmetric* (see e.g. Ref. [106]). If that mechanism generates similar asymmetries, then the coincidence of Eq. (4.1) further suggests that DM might have a mass at the GeV scale. These asymmetries can be simultaneously generated in a *cogenesis* scenario or they can be transferred in different ways, which fall mainly into two categories: (dark) electroweak sphalerons and higher-dimensional or renormalizable operators.

In the darkogenesis model of Ref. [68], that is the starting point of this Chapter, one of these operators connect the neutron with the DM particles, that from now on we will call χ, with the neutron:

$$\mathcal{O}_6 = \frac{\chi udd}{\Lambda^2} \tag{4.2}$$

where Λ is the mediator mass scale. Below the QCD confinement scale (around 100 MeV), we obtain the unique relevant operator that could mix χ with the neutron n:

$$\mathcal{L}_{mix} = -\delta m\, \bar{n}\chi + \text{h.c.} \tag{4.3}$$

where δm is the mass mixing term. The existence of this operator, and thus the mixing between the nuetron and DM, has been suggested as a possible solution [107] to the neutron lifetime anomaly, namely the discrepancy between the measurement of the neutron lifetime from bottle measurements and beam measurements [108].

In Ref. [68] it was pointed out that it is possible to generate the baryon asymmetry at low temperatures around 30 MeV via oscillations between χ and n that are resonantly enhanced by finite-temperature effects. Therefore, we have a new asymmetry transfer mechanism between the dark and the visible sectors. We will illustrate this idea in a dark sector with a $U(1)'$ gauge symmetry.

4.2 Generation of the baryon asymmetry

4.2.1 The model

In Ref. [109], it was proposed a simple model that could address the discrepancy between the neutron lifetime measured from trapped neutrons versus those decaying in flight by opening up a new decay channel $n \to \chi A'$, where χ is a dark Dirac fermion, which can constitute a dark matter candidate, and A' is a dark photon. The low-energy effective Lagrangian is given by:

$$\begin{aligned}\mathcal{L}_{eff} = \bar{\chi}(iD - m_\chi)\chi + \bar{n}(i\partial - m_n + \mu_n \sigma^{\mu\nu} F_{\mu\nu})n - \frac{1}{4}F'_{\mu\nu}F'^{\mu\nu} \\ -\frac{1}{2}m^2_{A'}A'^{\mu}A'_{\mu} - \delta m \bar{n}\chi - \frac{\epsilon}{2}F_{\mu\nu}F^{\mu\nu} + \text{h.c.}\end{aligned} \tag{4.4}$$

where $D_\mu = \partial_\mu - ig'A'_\mu$ is the covariant derivative, with g' the gauge coupling, μ_n is the neutron magnetic moment and $F'^{\mu\nu}$ is the field strength tensor for the dark $U(1)'$ gauge interaction. We point out that χ is assumed to be a Dirac fermion since if χ is a Majorana fermion then, in UV models, it is not stable beacuse it would generically lead to dinucleon decays such as $^{16}\text{O}(pp) \to^{14} \text{C}\pi^+\pi^-$ [110].

In Ref. [68], it was pointed out that the same model can also provide a low-scale realization of baryogenesis, if suitably augmented with dark fermions and radiation in order to be consistent with cosmological bounds. However, as stressed by the same authors, using the much simpler original version of the model, presented in Eq. (4.4), it is possible to explain the baryon asymmetry, giving up, however, the possibility to explain the neutron lifetime anomaly.

Experimental constraints on the Kinetic Mixing Parameter In Eq. (4.4), the last term kinetically mixes the photon of QED with the dark photon associated to the $U(1)'$ gauge symmetry. The mixing parameter ϵ is, in principle, a free parameter of the theory since the above mixing term is a gauge invariant, renormalizable operator [111]. Here we summarise the constraints on ϵ for the masses of our interests.
An upper bound comes from direct detection experiments measuring the scattering interactions of DM off protons, with cross section:

$$\sigma_{\chi,P} = \frac{4\alpha(g'\epsilon)^2\mu_{p\chi}^2}{m_{A'}^4} \tag{4.5}$$

where $\mu_{p\chi}$ is the reduced mass of χ and the proton. The CRESST-III experiments sets the limit $g'\epsilon \lesssim 1.2 \times 10^{-7}$ [112]. More constraining limits come from beam dump experiments, where dark photons can be produced via bremsstrahlung when a high-intensity beam of particles in sent on a fixed target and they are detected via the leptons they decay into. The experiments at Orsay and E137 at SLAC [113] limit $\epsilon \gtrsim 1.5 \times 10^{-5}$ or $\epsilon \lesssim 4.2 \times 10^{-8}$ [114]. Moreover, further constraints on the kinetic mixing come from the observation of the neutrino flux from supernova 1987A, which sets $\epsilon \gtrsim 4.7 \times 10^{-8}$ or $\epsilon \lesssim 3.2 \times 10^{-10}$ [115].

Decoupling SM-Dark Sector It will be useful for later to give an estimate for the chemical decoupling condition of the kinetic mixing operator from the Standard Model interactions. The kinetic mixing term can be diagonalised by a field redefinition of the form:

$$A^\mu \to A^\mu - \epsilon A^{\mu'} \Longrightarrow eA_\mu J^\mu_{EM} \to eA_\mu J^\mu_{EM} - \epsilon e A'_\mu J^\mu_{EM} \tag{4.6}$$

where e is the usual QED electric charge and J^μ_{EM} is the electromagnetic current. The relevant process is $\gamma\,\gamma' \to e^+\,e^-$. If we assume that $T_{dec} \gg m_{A'}$, then we can estimate the cross section as:

$$\sigma v \sim \frac{2}{\pi^2} T^3 \tag{4.7}$$

In the above limit, the density of dark photons in the plasma can be estimated as:

$$n_{A'} \simeq \frac{2}{\pi^2} T^3 \tag{4.8}$$

where the factor 2 represents the number of degrees of freedom of the dark photon in the unbroken phase. The interaction rate Γ is therefore given by:

$$\Gamma \sim n_{A'} \sigma v \sim \frac{2}{\pi^2} T^3 n_{A'} \sigma v \sim \frac{2}{\pi^2} T^3 = \frac{\epsilon^2 e^4}{2\pi^3} T \tag{4.9}$$

To see if we are in kinetic equilibrium with the Standard Model, we have to compare Γ with the Hubble rate, which is given by:

$$H = \frac{T^2 g_*^{1/2}}{M_{Pl}} \frac{\pi}{\sqrt{30}} \tag{4.10}$$

where g_* is the number of degrees of freedom (for the temperatures that we will later consider $g_* = 10.25$) and $M_{Pl} = 2.4 \times 10^{18}$ GeV. Therefore:

$$\frac{\Gamma}{H} \sim \frac{e^4 \epsilon^2}{2\pi^3} T \frac{M_{Pl}}{T^2 g_*^{1/2}} \sim \frac{10^{-3}}{\pi g_*^{1/2}} \left(\frac{\epsilon}{10^{-10}} \right)^2 10^{-20} \times 2.4 \times 10^{18} \frac{\text{GeV}}{T} \sim \frac{10^{-5}}{g_*^{1/2}} \frac{\text{GeV}}{T} \tag{4.11}$$

If we look at temperatures that are interesting for the PTAs signal, let's say $T \sim 10$ MeV, we have:

$$\frac{\Gamma}{H}(T \sim 10\,\text{MeV}) \sim 10^{-6} \frac{\text{GeV}}{10\,\text{MeV}} \sim 10^{-4} \tag{4.12}$$

We learn that, when the dark $U(1)'$ PT happens, the SM is chemically decoupled from the Dark Sector.

4.2.2 Baryogenesis: theoretical framework

The oscillations of χ into neutrons is controlled by a 2×2 Hamiltonian in the $\chi - n$ space:

$$\mathcal{H} = \begin{pmatrix} \Delta E_n + m_n & \delta m \\ \delta m & \Delta E_\chi + m_\chi \end{pmatrix} \tag{4.13}$$

where δm is the mass mixing term in Eq. (4.3), m_n and m_χ are the masses of the neutron and of χ, respectively. ΔE_n is the mass shift of the neutron due to its elastic scattering on pions and it can be computed in different ways, but the most reliable technique use dispersion relations, combined with experimental data, as in Ref. [116, 117]. The results are presented in Fig. 4.1.

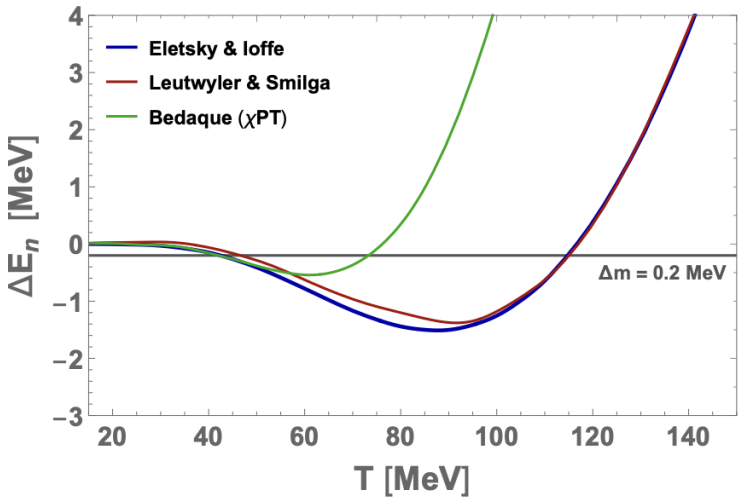

Figure 4.1: Thermal mass shift ΔE_n from dispersion relations (blue line [117], red line [116]) and chiral perturbation theory (green line [118]).Figure reproduced from Ref. [68].

ΔE_χ is the mass shift of DM χ due to the elastic scattering of χ on dark photons. Following the technique of Ref. [119], one obtains [68]:

$$\Delta E_\chi = g'^2 \frac{T_{A'}^2}{m_\chi} = g'^2 \frac{\xi^2 T^2}{m_\chi} \tag{4.14}$$

Here we have introduce the ratio of the temperature between the two sectors:

$$\xi = \frac{T_{A'}}{T} \tag{4.15}$$

We know that $\xi < 1$ and it is independent of the details of the UV physics, since the dark and the visible sectors are kinetically decoupled, as shown in Ref. [68].

We find the mixing angle θ by diagonalizing the Hamiltonian (4.13):

$$\tan(2\theta) = \frac{2\delta m}{\Delta m + \Delta E_n - \Delta E_\chi} \equiv \frac{2\,\delta m}{\delta E} \tag{4.16}$$

where $\Delta m \equiv m_n - m_\chi$. We define the difference between the eigenvalues:

$$|\delta\omega| = \sqrt{(\delta E)^2 + 4\,\delta m^2} \tag{4.17}$$

To find the efficiency of $\chi - n$ oscillations, let's use first simple quantum mechanical arguments. Suppose that we start with a state $\psi(t=0)\rangle = |\chi\rangle$ and we

evolve it with the Hamiltonian (4.13), leading to:

$$|\psi(t)\rangle = e^{-i(\omega_1+\omega_2)t/2}\left[\left(\cos\frac{\delta\omega}{2}t - i\cos 2\theta\sin\frac{\delta\omega}{2}t\right)|\chi\rangle - i\left(\sin 2\theta\sin\frac{\delta\omega}{2}t\right)|n\rangle\right] \tag{4.18}$$

Therefore the probability of oscillating into a neutron is given by:

$$P_n(t) = \sin^2(2\theta)\sin^2(\delta\omega\, t/2) \tag{4.19}$$

However we have to consider that the neutrons interact with the pions in the bath, therefore there might not be enough time to fully oscillate. Therefore, one usually carries out a time average over the short time scale $1/\Gamma_n$, where Γ_n is the rate of interactions of neutrons on the heat bath of pions:

$$\bar{P}_n = \Gamma_n\int_0^\infty dt\, e^{-\Gamma_n t}P_n(t) = \frac{2\delta m^2}{\delta\omega^2+\Gamma_n^2} \tag{4.20}$$

where $\sin^2 2\theta = \delta m^2/(\delta m^2 + \delta E^2/4)$. The rate Γ_n is given by:

$$\Gamma_n = n_\pi\langle\sigma_{n\pi}v\rangle \tag{4.21}$$

where n_π is the thermal density of pions. The thermal average velocity $\langle v\rangle$ is computed as:

$$\langle v\rangle = \sqrt{\frac{8T}{(\pi m_\pi)}} \cong 1.6\frac{T}{m_\pi} \tag{4.22}$$

The cross section for neutrons to scatter on pions at low energy is [120, 121]:

$$\sigma_{n\pi} = 4\pi a_0^2 \cong \frac{0.1}{m_\pi^2} \cong 2\,\text{mb} \tag{4.23}$$

where the contributions from the $I = 1/2$ and $3/2$ isospin scattering lenghts are averaged as $\sigma = 4\pi(a_{1/2}^2 + 2a_{3/2}^2)/3$.

Ignoring the elastic scattering rate Γ_χ of DM on dark photons and scalar, which is very small, the rate of production of neutrons via oscillations per χ particle, is given by:

$$\Gamma_{\text{osc}} = \bar{P}_n\Gamma_n \tag{4.24}$$

Similarly,the rate of production of χ per neutron must proceed with the same rate, therefore the number density of χ decreases as:

$$\dot{n}_\chi = -\Gamma_{\text{osc}}(n_\chi - n_n) \tag{4.25}$$

In our model, χ carries baryon number $B_\chi = +1$ and the total baryon number is conserved, therefore the quantity $n_\chi + n_n$ is conserved. If we define:

$$f = \frac{n_n}{n_n + n_\chi} \tag{4.26}$$

as the fraction of DM converting to neutrons, then:

$$\dot{f} = \Gamma_{\rm osc}(1 - 2f) \tag{4.27}$$

which has the solution:

$$f = \frac{1}{2}\left(1 - \exp\left(-2\int dt\Gamma_{\rm osc}\right)\right) \cong \frac{1}{2}\left(1 - \exp\left(-2\int \frac{dT}{T}\frac{\Gamma_n \bar{P}_n}{H}\right)\right) \tag{4.28}$$

provided that $P_{\rm osc} < 1$. Here we adopt the following definitions: $H = \rho_{rad}\frac{1}{3M_{pl}}$,$M_{pl} = 2.4 \times 10^{18}$ GeV and $g_* \cong 10.75$. We notice that:

$$\frac{\Omega_\chi}{\Omega_B} \cong 5.3 \Leftrightarrow \frac{1-f}{f} \cong 5.3 \tag{4.29}$$

which implies that we need:

$$f \cong 0.16 \tag{4.30}$$

We define the resonance temperature T_r for which δE, which is dependent on the thermal corrections, is equal to zero, i.e. $\delta E(T_r = 0)$. At T_r the mixing is maximal, although the oscillation probability is reduced by the damping from Γ_n, as in Eq. (4.20). Now let us look at the integrand of Eq. (4.28). At T_r this quantity will peak, therefore the baryon number generation will be dominated by the resonant oscillations between χ and n. An example is presented in Figure 4.2.

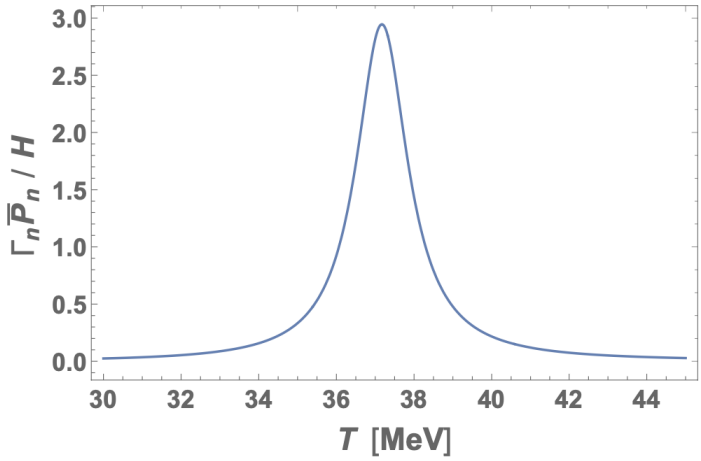

Figure 4.2: The integrand of Eq. (4.28), which represents the efficiency of the DM conversion into neutrons, versus the photon temperature T, using $\Delta m = 0.105$ MeV and $\delta m = 1.05 \times 10^{-10}$ MeV. In this case, the resonance temperature is $T_r \simeq 37\,\text{MeV}$, for which we have renonant oscillations between χ and n. Figure taken from [68].

In particular, the efficiency of the baryon asymmetry production, i.e. the integrand in Eq. (4.28), will scale as $\delta m^2/\Gamma_n$.

Boltzmann equations

A more rigorous way to study the relative abundances of χ and n is provided by the density matrix formalism, as prescribed in Refs. [122, 123]. We define a 2×2 matrix, whose diagonal entries represent the number densities n_n and n_χ, while the off-diagonal entries correspond to the superposition of quantum states originated by the oscillations. As it is usually done, we introduce the comoving densities $Y \equiv n/s$, where s is the total entropy density of the Universe. We follow the evolution in terms of the independent, dimensionless variable $x \equiv m_n/T$. Therefore, we introduce the comoving number density matrix:

$$Y(x) = \begin{pmatrix} Y_{11}(x) & Y_{12}(x) \\ Y_{21}(x) & Y_{22}(x) \end{pmatrix} \tag{4.31}$$

where $Y_{11} \equiv Y_n$, $Y_{22} \equiv Y_\chi$, $Y_{12} \equiv Y_{11} + Y_{22}$,$Y_{21} \equiv Y_{11} - Y_{22}$.
The evolution equation for the density matrix Y reads:

$$\frac{dY}{dx} = -\frac{i}{Hx}[\mathcal{H}, Y] - \frac{\Gamma_n}{2Hx}[P_n, [P_n, Y]] - \frac{\Gamma_\chi}{2Hx}[P_\chi, [P_\chi, Y]] \tag{4.32}$$

where $P_{n,\chi}$ are the projectors over the neutron or DM, respectively. On the right hand side, the first term accounts for oscillations, while the other two for the scattering processes in the thermal plasma. Eventually one obtains:

$$\frac{dY}{dx} = -\frac{i}{Hx}\begin{pmatrix} -\delta m\, Y_- & -\delta m\, \delta Y + \delta E\, Y_{12} \\ \delta m\, \delta Y - \delta E\, Y_{21} & \delta m\, Y_- \end{pmatrix} - \frac{\Gamma_n + \Gamma_\chi}{2Hx}\begin{pmatrix} 0 & Y_{12} \\ Y_{21} & 0 \end{pmatrix} \tag{4.33}$$

where we have defined $\delta Y \equiv Y_{11} - Y_{22} = Y_n - Y_\chi$, $Y_\pm = Y_{12} \pm Y_{21}$. In the following, as we have done before, we will neglect Γ_χ since it is much smaller than Γ_n.
We will recast the equations in terms of δY,Y_+ and $\eta \equiv i\delta m\, Y_-$:

$$\delta Y' = \frac{2}{Hx}\eta_-, \tag{4.34}$$

$$\eta_-' = \frac{\delta m}{Hx}(-2\delta m\, \delta Y + \delta E\, Y_+) - \frac{\Gamma_n}{2Hx}\eta_-, \tag{4.35}$$

$$Y_+' = -\frac{\delta E}{\delta m\, Hx}\eta_- \tag{4.36}$$

We integrate this system with initial conditions $Y_{22} = Y_X^\infty$ and $Y_{ij} = 0$ for the other components. Since $Y_{11} + Y_{22}$ is conserved, the fraction of DM that converts to neutrons is:

$$f = \frac{Y_{11}}{Y_\chi^\infty} = 1 - \frac{Y_{22}}{Y_\chi^\infty} \tag{4.37}$$

4.2.3 Parameter space

We can plot in the $\delta m - \Delta m$ plane the parameter space that reproduces the correct baryon asymmetry, as in Figure 4.3. As we have noticed before, the baryon asymmetry will scale as $\delta m^2/\Gamma_n$. If we increase Δm, the resonance temperature will increase, and so will Γ_n, because of the higher density of pions. This implies that δm must increase with Δm to keep the baryon asymmetry constant.
Therefore the baryon asymmetry depends mainly on Δm and δm, with a weak dependence on the combination $g'\xi$.

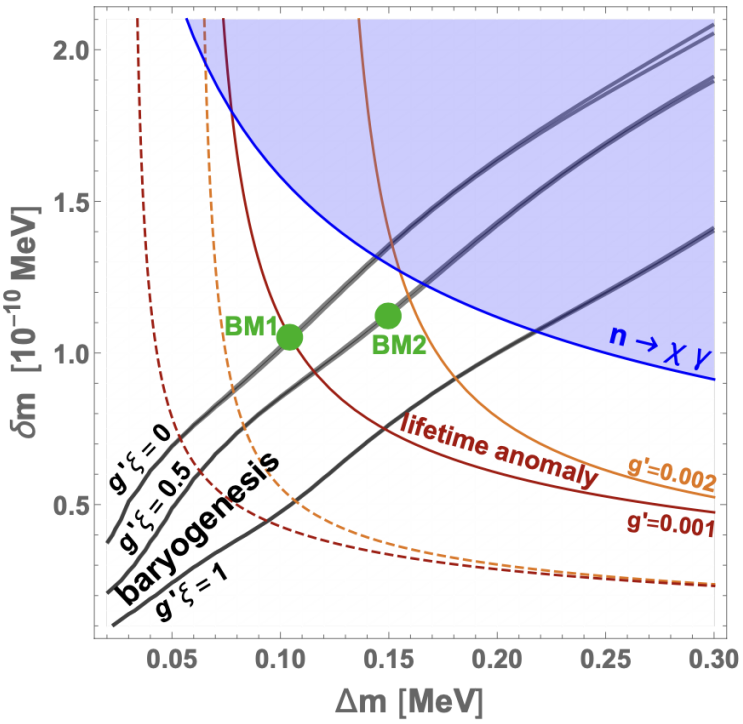

Figure 4.3: Parameter Space of the model presented in Ref. [68] in the $\delta m - \Delta m$ plane, where δm is the mass mixing term and $\Delta m = m_n - m_\chi$. The black solid lines give the observed baryon asymmetry for different values of $g'\xi$. The blue shaded area is excluded from $n \to \chi\gamma$ The red (orange) solid lines indicate the values of δm to explain the neutron lifetime anomaly, assuming $m_{A'}/g' = 60$MeV for $g' = 0.002(0.001)$, while the red (orange) dashed lines are obtained using $m_{A'}/g' = 30$MeV instead. For more details, see the main text.

The black contours give the correct baryon asymmetry, i.e. Eq (4.30), for different values of $g'\xi$ using both Eq (4.28) and (4.37). The difference between the predictions obtained using the two different equations is small, therefore showing a good agreement between the two different approaches. The blue area is excluded from the null searches for the decay $n \to \chi\gamma$, whose branching ration must be $\lesssim 0.17$ times the 0.9% needed to resolve the lifetime discrepancy [124]. This implies:

$$\delta m \lesssim 5 \times 10^{-11}\,\text{MeV}\left(\frac{11\,\text{MeV}}{\Delta m}\right)^{1/2} \tag{4.38}$$

We find that $\Delta m \lesssim 0.2$ MeV to generate the correct baryon asymmetry, as can been easily seen in Figure 4.3.

In Fig. 4.3 there are two different benchmark points, named BM1 (whit $\Delta m =$

$0.105\,\mathrm{MeV}$, $\delta m = 1.05 \times 10^{-10}\,\mathrm{MeV}$) and BM2 (with $\Delta m = 0.15\,\mathrm{MeV}$, $\delta m = 1.12 \times 10^{-10}\,\mathrm{MeV}$), that reproduces the baryon asymmetry. In the former case, the values $g' = 0.001\,(0.002)$ are chosen such that the same model, augmented with new interactions in the dark sector, is able to also solve the neutron lifetime anomaly. For more details, again we refer the reader to Ref. [109].

4.3 $U(1)'$ Phase Transition

4.3.1 The UV model

We want to build a UV model that in the low-energy limit reproduces the Lagrangian (4.4), following Ref. [109]. We demand that the mass of the dark photon originates via the Higgs mechanism, when the complex scalar ϕ gets its VEV. The terms of the Lagrangian are constrained by the gauge symmetries of the theory. In order to have renormalizable interaction of χ with the quarks, we introduce a triplet scale Φ_1, which is also charged under $U(1)'$. Moreover, we introduce a second triplet scalar Φ_2, neutral under $U(1)'$ which couples to other quarks in the neutron and we need to introduce a trilinear scalar interaction:

$$\mu \Phi_{1,a} \Phi_2^{*a} \phi \tag{4.39}$$

where μ is a constant with unit mass. Finally, to satisfy the $SU(2)_L$ symmetry, the scalar triplets couple only to the right-handed quarks:

$$\lambda_1 \bar{d}^a P_L \chi \Phi_{1,a} + \lambda_2 \epsilon^{abc} \bar{u}_a^C P_R d_b \Phi_{2,c} \tag{4.40}$$

where λ_1 and λ_2 are two dimensionless coupling constants. The triplet scalars can decay into two jets or a jet plus missing energy and then, to satisy LHC constraints on their detection, their mass should be larger than about a TeV [125]. Therefore we can integrate them out, obtaining the following effective operator:

$$\frac{\lambda_1 \lambda_2 \mu}{m_{\Phi_1}^2 m_{\Phi_2}^2} \phi \, \epsilon^{abc} (\bar{u}_a^C P_R d_b)(\bar{\chi} P_R d_c) \tag{4.41}$$

When ϕ gets a VEV, the above term fixes the coefficient of the $n - \chi$ oscillations:

$$\delta m = \frac{\lambda_1 \lambda_2 \beta \langle \phi \rangle \mu}{m_{\Phi_1}^2 m_{\Phi_2}^2} \sim 10^{-10}\,\mathrm{MeV} \tag{4.42}$$

where $\beta = 0.014\,\mathrm{GeV}^3$ from the lattice matrix element $\langle 0|udd|0\rangle$ [126].

4.3.2 Scale-invariant potential and phase transition

So far, we have reviewed the model as presented in [68]. We now introduce a novelty with respect to [68], i.e. we assume that the potential of the scalar ϕ is classically scale invariant, i.e. without a bare mass term, and that the VEV of ϕ arises from the radiative corrections, as in the original Coleman-Weinberg model [90]. Namely, the potential is:

$$V = \lambda\phi^4 \tag{4.43}$$

We will now compute the one-loop corrections to the potential à la Coleman-Weinberg, introducing the constant field background ϕ_c. The full details of the computation of the Effective Potential are reported in Appendix A.
Since we have integrated the heavy scalar triplets out, they will not contribute to the calculation and we are left with the contributions from the scalar ϕ and the gauge boson A'. We write the complex scalar in terms of its real and imaginary component:

$$\phi = \frac{\varphi_r + \varphi_i + \phi_c}{\sqrt{2}} \tag{4.44}$$

The field-dependent masses for the real and imaginary components of ϕ are, respectively:

$$m_r^2(\phi_c) = 3\lambda\phi_c^2 \tag{4.45}$$
$$m_i^2(\phi_c) = \lambda\phi_c^2 \tag{4.46}$$

while for the gauge boson A' we have:

$$m_{A'}^2(\phi_c) = g'^2\phi_c^2 \tag{4.47}$$

In the end, the one-loop effective potential at $T = 0$, computed using the dimensional regularization and the $\bar{\text{MS}}$ renormalization scheme, is:

$$\begin{aligned} V_{eff}(\phi_c) = \lambda\phi_c^4 + \frac{1}{64\pi^2}\Bigg[3m_{A'}(\phi_c)^4\left(\log\frac{m_{A'}^2(\phi_c)}{M^2} - \frac{5}{6}\right) \\ +m_r^4(\phi_c)\left(\log\frac{m_r^2(\phi_c)}{M^2} - \frac{3}{2}\right) + m_i^4(\phi_c)\left(\log\frac{m_i^2(\phi_c)}{M^2} - \frac{3}{2}\right)\Bigg] \end{aligned} \tag{4.48}$$

where M in an arbitrary renormalization scale, which has not an effect on the physics of the model. Indeed, if we change the renormalizaion scale in $M \to M'$, we can always redefine the coupling constants and the potential: it is a change in the parametrization, not in the physics.
Following the method in Ref. [90], since M is arbitrary, we can choose it to be at the location of the minimum, $\langle\phi\rangle = \frac{v}{\sqrt{2}}$. Therefore, by imposing that:

$$V'(\langle\phi\rangle) = 0 \tag{4.49}$$

we find the values of λ for which we have the desired minimum, yielding the necessary δm for the generation of the baryon asymmetry below the GeV scale, as shown in Eq. 4.42. In Fig. 4.4 we show, as an example, the plot of the Effective Potential at one-loop for $v = 60\,\text{MeV}$ and $g' = 0.6$.

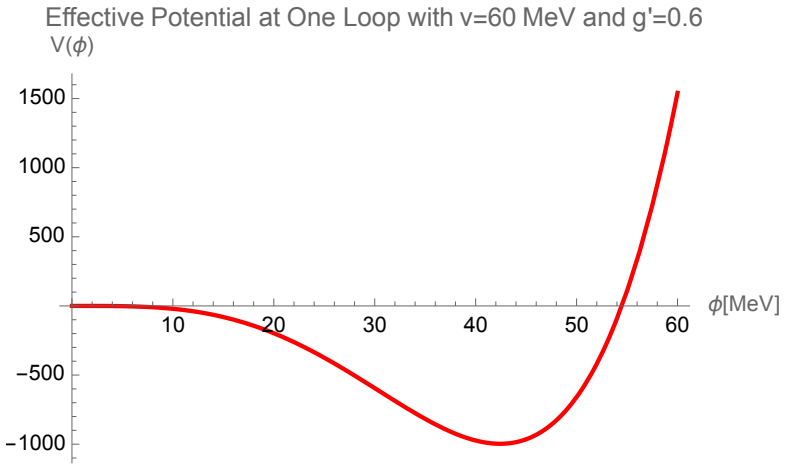

Figure 4.4: Effective Potential at One-Loop given by Eq. (4.48) for $v = 60$ MeV, $g' = 0.6$ and λ computed as prescribed in the main text, using the condition Eq. (4.49).

After symmetry breaking, the VEV of ϕ gives the dark photon a mass such that:

$$\frac{v}{\sqrt{2}} = \frac{m_{A'}}{g'} \tag{4.50}$$

Constraints on the values of v come from neutron stars: the mixing between n and χ allows the former to convert in DM, softening the Tolman-Oppenheimer-Volkoff equations, which determine the structure of neutron stars, such that the possible maximal mass of a neutron star is lower than the largest observed masses, close to $2M_\odot$. A possible solution is given by repulsive self-interactions between DM, which could arise in our model as Coulombian repulsion since χ is charged under $U(1)'$. In Ref. [109] it was computed that it is possible to obtain a $2M_\odot$ mass neutron star if:

$$\frac{m_{A'}}{g'} \lesssim 45 - 60\,\text{MeV} \tag{4.51}$$

By direct computation, we find that the generation of the desired VEV depends critically on the value of g'. If the values of g' are very small, i.e. $g' \sim 10^{-3}$, we can't find real values of λ that generate the required VEV to explain the baryon asymmetry, therefore excluding the possibility of reproducing the baryon asymmetry for the values of the line $g'\xi = 0$ in Figure 4.3. For the same reason,

the values $g' \sim \mathcal{O}(10)$, which would place us on the line $g'\xi = 1$, are not a viable option.
On the other hand, considering $g'\xi = 0.5$, hence $g' > 0.5$, we are able to find small values of λ such that the radiative corrections generate the required VEV. The results are represented in Figure 4.5 for $v = 60$ MeV.

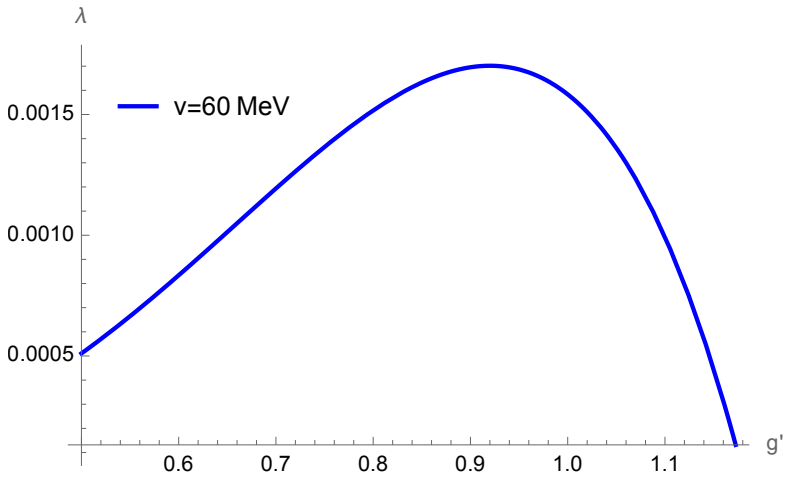

Figure 4.5: Values of λ_ϕ as a function of the gauge coupling g' that allow the generation the VEV of the Dark Higgs scalar $\langle\phi\rangle = v/\sqrt{2}$ such that we generate the correct value of the baryon asymmetry. Here we take $v = 60\,\text{MeV}$

4.4 Gravitational Wave Signal

The formation of a deeper, true minimum of the potential due to the interaction within the dark sector leads to the decay of the false vacuum, hence a phase transition occurs. This is the famous Coleman-Weinberg model [90], which provides a simple weakly-coupled realization of a supercooled phase transition. Therefore, we can now compute the parameters that characterize the phase transition, as introduced in Section 3.3: the nucleation temperature T_{nuc}, the strength of the phase transition α and the timescale of the phase transition β_H. Here we will not compute the wall velocity v_w.

4.4.1 Finite temperature corrections

A potential that leads to a supercool phase transition is flat around the origin and the finite temperature effects become important [127]. More in general, if we want to compute the tunnelling potential, we consider the full temperature

dependent potential, where the finite temperature corrections are given by Eq. (3.31). However, the problem is actually simpler at small temperatures and we can avoid computing the correction as in Eq. (3.31), since the dynamics of the phase transitions can be described using the high temperature expansion, as we will discuss more in detail later. In our model, we only need to consider the contribution from the gauge boson, since the contributions from the scalar are negligible with respect to the gauge boson because of the smallness of the quartic coupling λ. If the gauge coupling is the only relevant coupling of the model, then, using Eq. (3.33), we can write the potential at finite temperature as follows :

$$V_{T\neq 0}(\phi) = 3\frac{m_{A'}^2}{64\pi^2}\log\frac{m_{A'}^2}{M^2} - 3\frac{m_A^{'2}}{64\pi^2}\log\left(\frac{m_{A'}^2}{T^2\,a_b}\right) - \frac{1}{4}m_{A'}^3\frac{T}{2\pi^2} + \frac{1}{8}g^{'2}T^2\phi^2 \quad (4.52)$$

where the last three terms are the thermal corrections and we have defined $m_{A'} \equiv m_{A'}(\phi)$ to simplify the notation. We recall that $a_b = \pi^2\, e^{3/2-2\gamma_E}$, where γ_E is the Euler-Mascheroni constant.
Now let us focus on the logarithmic terms of the above expression. We can simplify the expression in the following way:

$$3\frac{m_A^{'2}}{64\pi^2}\log\frac{m_{A'}^2}{M^2} - 3\frac{m_A^{'2}}{64\pi^2}\log\left(\frac{m_{A'}^2}{T^2\,a_b}\right) = -3\frac{m_A^{'2}}{64\pi^2}\log\left(\frac{M^2}{T^2\,a_b}\right) \quad (4.53)$$

We define the energy scale:

$$B = \frac{M}{\sqrt{a_b}} \quad (4.54)$$

Here we notice that any logarithmic dependence on the field disappeared because of the cancellation between the logarithmic piece due to radiative corrections and the logarithmic piece in the high temperature expansion of the thermal functions. This is a common feature of the potentials that lead to a supercool phase transitions. We recall that M is an arbitrary renormalization scale, which we decide to set it to the vacuum expectation value of the field. In the end, we can define:

$$m^2(T) = \frac{1}{4}g^{'2}T^2 \quad (4.55)$$

$$\delta(T) = \frac{3}{4\pi}g^{'3}T \quad (4.56)$$

$$\lambda(T) = \frac{3}{8\pi^2}g^{'4}\log\left(\frac{T}{B}\right) \quad (4.57)$$

and rewrite the potential as follows:

$$V(\phi) = \frac{1}{2}m^2(T)\phi^2 - \frac{\delta(T)}{3}\phi^3 + \frac{\lambda(T)}{4}\phi^4 \quad (4.58)$$

The relevant effect of the finite temperature corrections will be to introduce a quadratic positive curvature for $T > 0$, turning the local minimum into a local metastable minimum and ensuring that the transition is of the first order. Let us explain why it is a good approximation at small T. Let us take the logarithmic piece of the gauge boson in Eq. (4.48). We can write it in the following way:

$$\log\left(\frac{g'\phi}{\mu}\right) = \log\left(\frac{g'\phi}{\sqrt{a_b}T}\right) + \log\left(\frac{T\sqrt{a_b}}{\mu}\right) = \log\left(\frac{g'\phi}{\sqrt{a_b}T}\right) + \log\left(\frac{T}{M}\right) \tag{4.59}$$

For very small T, i.e. for large supercooling,the second term $\log(T/M)$ becomes large and it dominates over the other piece. The effective quartic coupling is negative and proportional to the logarithm, driving the tunnelling process. When the logarithm is large, the barrier ends at ϕ sufficiently small that the high temperature expansion is a good approximation, hence Eq. (4.48) is valid for our scopes [127].

4.4.2 Bounce solution

We are now ready to compute the nucleation temperature. As we have discussed in Chapter 3, the expression of the tunnelling rate per unit volume Γ depends on whether the nucleation of the bubbles of true vacuum are induced by thermal effects or by quantum effects, or, in other words, if the field tunnels via $O(3)$ or $O(4)$ solutions, respectively. It has been proven in Ref. [128] that, for the Coleman-Weinberg potential, the tunneling rate is dominated by $O(3)$. For the computation, we will follow the approach presented in Ref. [128].
We can write the nucleation condition Eq. (3.12) as follows:

$$\Gamma(T_{nuc}) = H^4(T_{nuc}) \Longrightarrow \frac{S_3}{T_{nuc}} = 4\log\frac{H}{T_{nuc}} \tag{4.60}$$

where we have considered the approximation:

$$\Gamma = T^4\, e^{-S_3/T} \tag{4.61}$$

where we have dropped the prefactor $(S_3/2\pi T)^{3/2}$, which allows us to derive analytical results, without significant changes in the results.
The bounce action can be written as a product of a single parameter dimensionless function $\tilde{S}_d(\kappa)$ and a scaling coefficient, which depends on a combination of the thermal mass, cubic or quartic couplings. To find the expression of the dimensionless action, we exploit the reparameterization invariance of the the bounce equation Eq. (3.4). We perform a rescaling of the field and a change of coordinates:

$$r \to L\rho \tag{4.62}$$

$$\phi \to \zeta\varphi \tag{4.63}$$

In this way we obtain the dimensionless action $\tilde{S}_d$ and the scalar potential $\tilde{V}$:

$$S_d = \zeta^2 \, L^{d-2} Z_\phi \tilde{S}_d \tag{4.64}$$

$$V(\phi) = \zeta^2 \, L^{-2} \, Z_\phi \tilde{V}(\varphi) \tag{4.65}$$

where Z_ϕ is the wave-function renormalization, which, for the weakly coupled theories $Z_\phi \simeq 1$, neglecting 1-loop correction to the wave function. Now, the above reparemeterization allows us to write the potential as a function of single parameter. If we take:

$$\zeta = \frac{m^2(T)}{\delta(T)}, \qquad \text{and} \qquad L = \frac{1}{m(T)} \tag{4.66}$$

the dimensionless potential derived from Eq. (4.58) reads:

$$\tilde{V}(\varphi, T) = \frac{1}{2}\varphi^2 - \frac{1}{3}\varphi^3 + \frac{\kappa(T)}{4}\varphi^4 \tag{4.67}$$

with:

$$\kappa(T) \equiv \frac{\lambda(T) m^2(T)}{\delta^2(T)} \tag{4.68}$$

where $-\infty < \kappa(T) < \kappa_c$, with $\kappa_c \equiv \kappa(T_c) = 2/9$ and T_c is the critical temperature. In our case, the expression of κ takes quite a simple form:

$$\kappa(T) = \frac{1}{6} \log\left(\frac{T}{B}\right) \tag{4.69}$$

The bounce solution can be deduced for all values of κ by fitting $\tilde{S}_3(\kappa)$ using analytical know solutions for special values of κ.
We can then relate $\tilde{S}_3(\kappa)$ with $S_3(T)$ via the relation:

$$S_3(T) = \frac{m^3(T)}{\delta^2(T)} \tilde{S}_3(\kappa) \tag{4.70}$$

by plugging Eq. (4.66) in Eq. (4.64). In the end, we obtain:

$$\frac{S_3}{T} \simeq \begin{cases} \frac{4\pi^3}{27 g'^3} \frac{1}{(k-k_c)^2} \bar{B}_3(\kappa) & \kappa > 0 \\ \frac{3\pi^3}{g'^3} \left(\frac{1+e^{-1/\sqrt{|k|}}}{1+\frac{9}{2}|\kappa|} \right) & \kappa < 0 \end{cases} \tag{4.71}$$

where we have defined:

$$\bar{B}_3(\kappa) \equiv \frac{16}{243} B_3^+(\kappa) \tag{4.72}$$

using the fitting function

$$B_3^+ = 1 - 38.23\left(\kappa - \frac{2}{9}\right) + 115.26\left(\kappa - \frac{2}{9}\right)^2 + 58.07\sqrt{\kappa}\left(\kappa - \frac{2}{9}\right)^2 + 229.07\kappa\left(\kappa - \frac{2}{9}\right)^2 \tag{4.73}$$

Since we expect the nucleation temperature T_n to be smaller than M, we consider the case $\kappa < 0$. Therefore,in vacuum domination, the nucleation condition Eq. (4.60) reads:

$$\frac{3\pi^3}{g^3}\left(\frac{1 + e^{-1/\sqrt{|k_n|}}}{1 + \frac{9}{2}|\kappa_n|}\right) = 4\log\left(\frac{B}{H_V}\right) - 24|\kappa_n| \tag{4.74}$$

where we have defined $\kappa_n \equiv \kappa(T_n) = 1/6\log(T_n/B)$ and H_V is the contribution to the Hubble rate due to the vacuum energy, namely:

$$H_V^2 = \frac{\Delta V_0}{3M_{pl}^2} \tag{4.75}$$

where ΔV_0 is the the potential energy difference between the two minima at zero temperature and $M_{pl} = 2.4 \times 10^{18}\,\text{GeV}$. Using Eq. (4.74), we can compute the nucleation temperature for the model. Here we want to point out that,in literature, there are other analytical formulas to compute the nucleation temperature (see e.g. Ref. [85, 129]), which, however, were derived without considering the cubic term in the high temperature expansion. Nevertheless, these formualas are valid only when $|k_n| \gg 1$, which is a situation that is not realized in our parameter space.

4.5 Results

4.5.1 Computation of the Phase Transition Parameters

We are now ready to compute the parameters of the phase transition.

Nucleation Temperature

We can compute the nucleation temperature using Eq. (4.74). The results of the nucleation temperature, as a function of the gauge coupling g', computed for different values of the VEV are represented in Figure 4.6

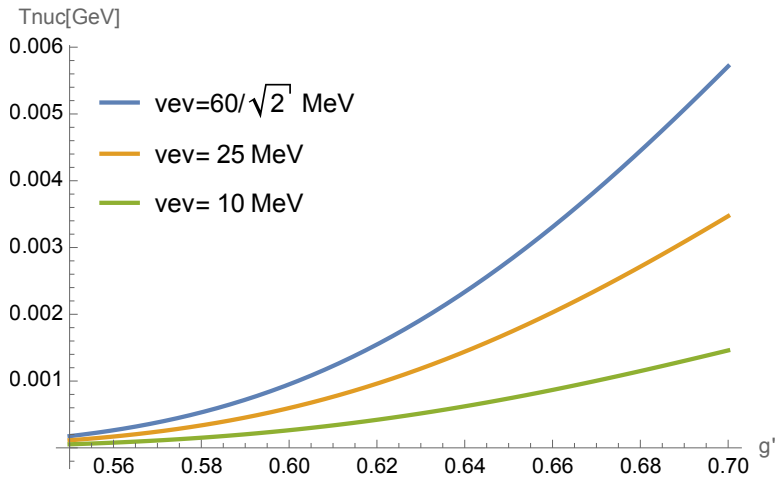

Figure 4.6: Nucleation temperature, as a function of the gauge coupling g'

Here we notice that for not all the values of the gauge coupling of the model presented in Section 4.3.1 we are able to achieve temperatures of the order of a $\mathcal{O}(0.1 - 10)$ MeV. In fact, the formula Eq. 4.74 breaks down above $g' \sim 0.7$ since the nucleation temperature will reach the value of the critical temperature and we will not be in vacuum domination, but rather in radiation domination.

Phase transition Strength α

We can compute the phase transition strength, using Eq. (3.15), that we rewrite here for our model:

$$\alpha = \frac{\Delta V_0}{\rho_{rad}(T_{nuc})} \tag{4.76}$$

where:

$$\rho_{rad}(T) = \frac{\pi^2 g_*}{30} T^4 \tag{4.77}$$

with $g_* = 10.25 + 2$, where we added two degrees of freedom, that come from the dark scalar ϕ in the unbroken phase,to the SM degrees of freedom. The results, as a function of the gauge coupling,are reported in Figure 4.7.

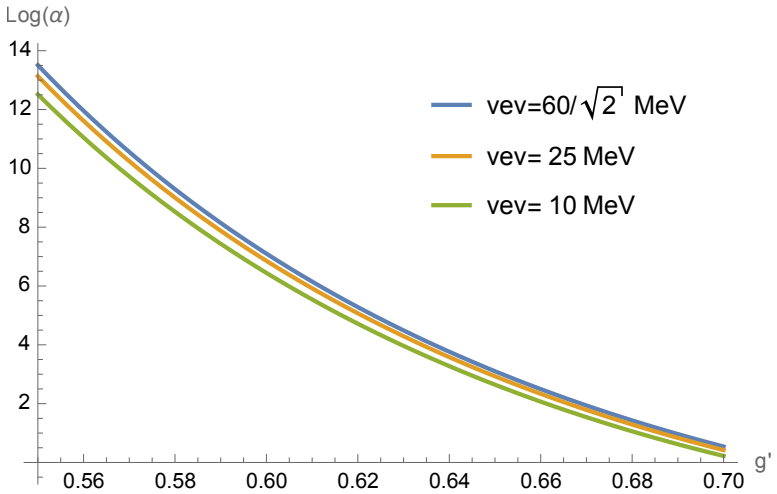

Figure 4.7: Phase transition strength, as a function of the gauge coupling g'

We see that the strength of the phase transition decreases exponentially with the gauge coupling.

Phase Transition Rate

The last parameter that we have to compute is the phase transition rate β_H. Since the $O(3)$ tunnelling rate is dominating, the formula will read:

$$\frac{\beta}{H_n} = T \left. \frac{d(S_3/T)}{dT} \right|_{T_{nuc}} \tag{4.78}$$

The results are reported in Figure 4.8.

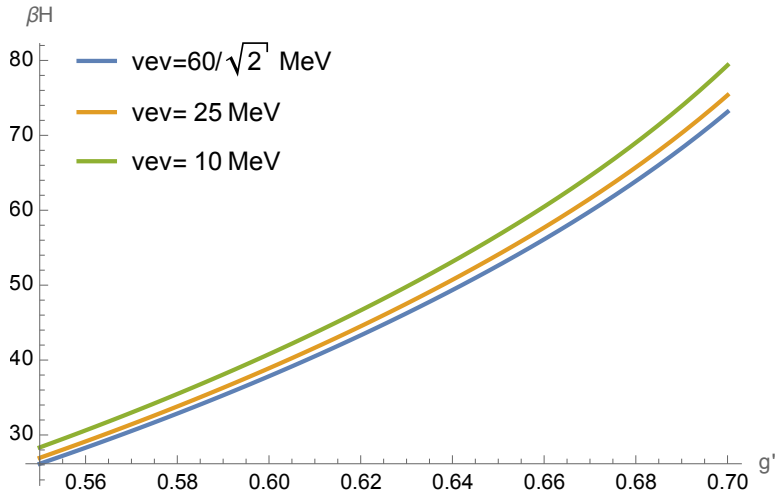

Figure 4.8: Phase transition rate, as a function of the gauge coupling g'

We notice that the duration of the phase transition decreases linearly with the gauge coupling.

4.5.2 Comparison with the PTAs data

Now that we have computed the thermodynamics parameters of the Phase Transition in our model, we can ask ourselves if they could be compatible with the GW signal observed at PTAs. By combining data from two or more PTAs data, the possibility of a FOPT generating the GW signal has been scrutinized in the last year, see. e.g. Ref. [130, 131].In particular, a general finding of the analysis in Ref. [131], is that the phase transition has to be strong or moderately strong, i.e. $\alpha \gtrsim 0.3$ and relatively slow, i.e. $\beta/H_n \lesssim 100$, in order to be compatible with the GW signal. The analysis in Ref. [131] is, to our knowledge, the most accurate analysis so far, since it combines data from three different PTAs collaborations (NANOGrav, PPTA and EPTA), while previous studies relied only on either one or two sets of data. Moreover, by means of a frequentist approach to the analysis, the results don't depend strongly on prior assumptions on the phase transition parameters, which was an issue of Bayesian analysis of the signal (see e.g. Ref. [132]).

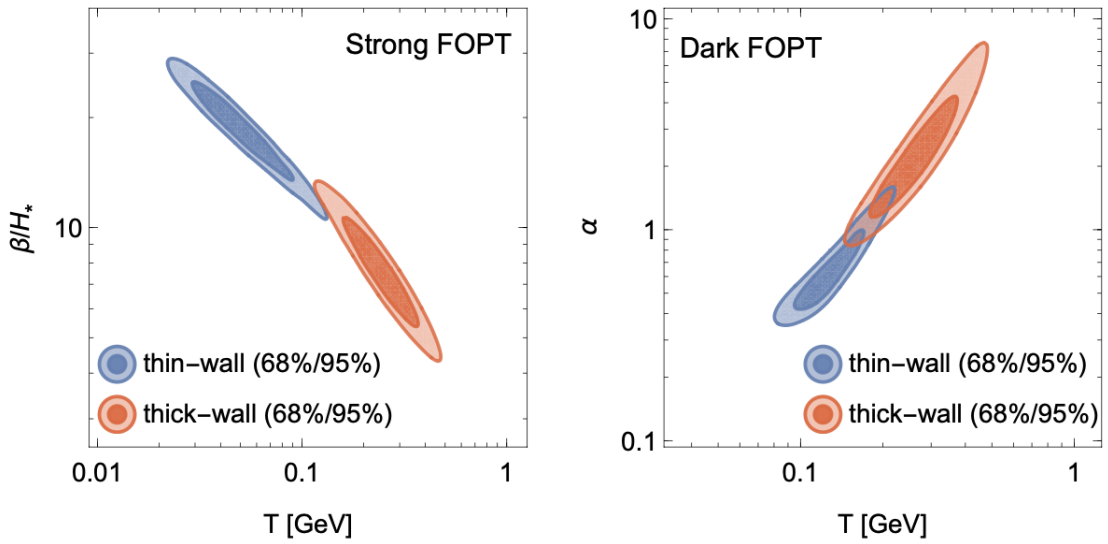

Figure 4.9: Confidence regions $(68\%, 95\%)$ for a strong FOPT (left panel) and a FOPT in a dark sector (right panel) from the fits of the PTAs signal in Ref. [131]. The fits were done by considering the thin-wall and the thick-wall regime of vacuum tunnelling. The confidence regions for these two regimes are showed separately in blue and orange, respectively. Figure taken from Ref. [131].

Therefore, our results are compatible with this analysis and offer an interesting staring point for a more sophisticated analysis of the parameter space of the model.

Chapter 5

Conclusions

In this thesis we have proposed a low scale baryogenesis model that relies on a $U(1)'$ supercooled phase transition that occurs below the GeV scale in order to explain the gravitational wave signal observed by pulsar timing arrays.

In Chapter 2, we have first reviewed the problem of the baryon asymmetry and explained the current and past baryogenesis theories. In particular, we have stressed why it is worth to explore low scale baryogenesis models: on the one hand, they are motivated by theories that predict a low reheating temperature, on the other hand they could be tested in different experimental facilities in the next decade.
In Chapter 3 we reviewed Cosmological First Order Phase Transitions, building the basic toolkit to study them. Moreover, we introduced supercooled phase transitions. We have provided two explicit realizations of BSM theories that lead to a FOPTs: an Effective Field Theory with a dimension 6 operator $|H|^6$ (where H is the SM Higgs doublet) and a theory with a strongly coupled sector, that gives rise to a light dilaton potential. For these two models we have computed the nucleation temperature and highlighted the difference between them: the light dilaton potential leads to a supercooled phase transition, and thus a different phenomenology with respect to the EFT-induced phase transition.
In Chapter 4 we have presented our original proposal. First we have reviewed the baryogenesis model presented in Ref. [68]. In the model, we introduce a dark Dirac χ dark matter candidate and a dark photon A', which obtains its mass from a dark $U(1)'$ Higgs mechanism. We go beyond Ref. [68] by supposing that the dark Higgs potential is classically scale invariant and that the VEV of the Dark Higgs, which the baryon asymmetry strongly depends on, gets generated via radiative corrections. This is the famous Coleman-Weinberg model, which gives rise to a supercooled phase transition. We find that for values of the VEV around or below ~ 42 MeV and gauge couplings $g' \lesssim 0.7$, the phase transition parameters

(T_{nuc}, α, β_H) could explain the GW signal observed last year by PTAs.

Our analysis can be improved in different ways. A possible improvement and test of the reliability of the results would be to compute the bounce solution, which enters in the computation of the parameters of the phase transition, by means of an original numerical code or existing numerical routines.
Furthermore, in order to constraint the parameter space of the model, it could be interesting to analyze the impact of the phase transition on BBN and the CMB. In fact, it is known (e.g. see Refs. [132, 133, 134]) that supercool phase transitions occuring around or below a few MeV can modify the number of relativistic effective degrees of freedom N_{eff}, subsequently changing the primordial abundances of light elements and the power spectra that are measured by the CMB experiments. Our results in Figure 4.6, show that the nucleation temperature can indeed be around or below a MeV, therefore a quantitative study of the parameter space satisfying BBN and CMB constraints could be a further direction of this work.

In conclusion, this work provided a new explanation of PTAs signal, connecting for the first time, the possible GW signal with the generation of the baryon asymmetry. Furthermore, this work shows how PTAs experiments, and more in general GWs observations, provide a new way to probe the dynamics of hidden sectors. In particular, we have provided a new way to test low scale baryogenesis models.

Appendices

Appendix A

The Effective Potential

Here we first review how to compute the effective action and the effective potential at one loop, following mainly Refs. [104, 135]. Then, we will illustrate the most important steps for the computation of our model in the main text.

A.1 Theoretical Framework

A.1.1 Effective Action and Effective Potential

Let's consider the Lagrangian density $\mathcal{L}(\Phi, \partial_\mu \Phi)$, describing the theory of a real scalar field Φ, which is coupled to an external source $J(x)$:

$$\mathcal{L} \to \mathcal{L} + J(x)\Phi(x) \tag{A.1}$$

The generating functional $Z[J]$ is usually written in terms of a functional $W[J]$ as:

$$Z[J] = \langle 0|0\rangle_J \equiv e^{iW[J]} = \int \mathcal{D}\Phi\, e^{i\int d^4x[\mathcal{L}(\Phi,\partial_\mu\Phi)+J\Phi]} \tag{A.2}$$

$W[J]$ is called the *connected generating functional* since its derivatives with respect to iJ at $J = 0$ give the connected Green's functions of the theory and it can be Taylor expandend as follows:

$$W[J] = \sum_n \frac{i^n}{n!} \int d^4x_1 \ldots d^4x_n\, G^{(n)}(x_1, \ldots, x_n) J(x_1) \ldots J(x_n) \tag{A.3}$$

where $G^{(n)}$ denotes the n- point connected Green's functions, which are computed as the sum of all connected Feynman diagrams with n external lines.

Now,consider the functional derivative of $W[J]$ with respect to $J(x)$:

$$\frac{\delta}{\delta J(x)} W[J] = i \frac{\delta}{\delta J(x)} \log Z = -\frac{\int \mathcal{D}\Phi\, e^{i\int(\mathcal{L}+J\Phi)}\Phi(x)}{\int \mathcal{D}\Phi\, e^{i\int(\mathcal{L}+J\Phi)}} \tag{A.4}$$

Then we define the *classical field* $\phi_c(x)$ as:

$$\phi_c(x) \equiv \frac{\delta}{\delta J(x)} W[J] = \frac{\langle 0|\Phi(x)|0\rangle_J}{\langle 0|0\rangle_J} \tag{A.5}$$

where the right hand side is the vacuum expectation value in the presence of a nonzero source $J(x)$.
We introduce the *effective action* $\Gamma[\phi_c]$ defined as Legendre transformation of $W[J]$:

$$\Gamma[\phi_c] = W[J] - \int d^4\, x\, J(x)\phi_c(x) \tag{A.6}$$

We can expand the effective action as follows:

$$\Gamma[\phi_c] = \sum_{n=0}^{\infty} \frac{1}{n!} \int dx_1 \dots dx_n\, \Gamma^{(n)}(x_1, \dots, x_n)\phi_c(x_1) \dots \phi_c(x_n) \tag{A.7}$$

The coefficients $\Gamma^{(n)}$ can be shown to correspond to the one-particle irreducible (1P1) Green's functions of the theory. Then we compute:

$$\frac{\delta\Gamma[\phi_c]}{\delta\phi_c} = \int d^4 y\, \frac{\delta W[J]}{\delta J(y)} \frac{\delta J(y)}{\delta\phi_c(x)} - J(x) - \int d^4 y\, \frac{\delta J(y)}{\delta\phi_c(x)}\phi_c(y) = -J(y) \tag{A.8}$$

or, equivalenty,

$$\left.\frac{\delta\Gamma[\phi_c]}{\delta\phi_c}\right|_{J=0} = 0 \tag{A.9}$$

The spontaneuos symmetry breaking takes place when the classical field that minimize the effective action is different from zero.
We can compute the effective action by expanding in powers of the external momenta, for which we need to consider the Fourier transforms of the functions $\Gamma^{(n)}(x_1, \dots, x_n)$ (which are the 1P1 Green functions):

$$\begin{aligned}\Gamma^{(n)}(x_1, \dots, x_n) = \int \frac{d^4 p_1}{(2\pi^4)} \dots \frac{d^4 p_n}{(2\pi^4)} e^{i(p_1 x_1 + \dots + p_n x_n)} \\ \times (2\pi)^4 \delta(p_1 + \dots + p_n)\tilde{\Gamma}^{(n)}(p_1, \dots, p_n)\end{aligned} \tag{A.10}$$

and expand $\tilde{\Gamma}^{(n)}$ in powers of momenta around $p_i = 0$:

$$\tilde{\Gamma}^{(n)}(p_1, \dots, p_n) = \tilde{\Gamma}^{(n)}(0) + \dots \tag{A.11}$$

Thus, the effective action reads:

$$\begin{aligned}\Gamma[\phi_c] = \sum_{n=0}^{\infty} \frac{1}{n!} \int dx_1 \dots dx_n\, \phi_c(x_1) \dots \phi_c(x_n) \int \frac{d^4 p_1}{(2\pi^4)} \dots \frac{d^4 p_n}{(2\pi^4)} e^{i(p_1 x_1 + \dots + p_n x_n)} \\ \times \int d^4 x\, e^{-ix(p_1 + \dots + p_n)} [\tilde{\Gamma}^{(n)}(0) + \dots] = \int d^4 x \sum_{n=0}^{\infty} \frac{1}{n!} \tilde{\Gamma}^{(n)}(0)\phi_c^n(x) + \dots\end{aligned} \tag{A.12}$$

The first term of the expansion is written as:

$$-\int d^4x\, V_{eff}(\phi_c) \tag{A.13}$$

where we finally define the *effective potential*:

$$V_{eff}(\phi_c) = -\sum_{n=0}^{\infty} \frac{1}{n!}\tilde{\Gamma}^{(n)}(0)\phi_c^n \tag{A.14}$$

The condition that $\Gamma[\phi_c]$ has an extremum is given by:

$$\frac{dV_{eff}(\phi_c)}{d\phi_c} = 0 \tag{A.15}$$

This result tells us that we can find the minimum of the theory, taking into account quantum corrections, via the minimization of a simple function.

The Background Field Method

Now we review how to compute the Effective Potential using the background field method. We consider the Lagrangian density for a scalar field Φ:

$$\mathcal{L}(\Phi, \partial_\mu\Phi) = \frac{1}{2}\partial_\mu\Phi\partial^\mu\Phi - V(\Phi) \tag{A.16}$$

where $V(\Phi)$ is the tree level potential. We write the scalar field Φ as the sum of a background field $\phi_c(x)$ and $\eta(x)$ as a dynamical field, accounting for the quantum fluactuations. The expontent of Eq. (A.2) takes the form:

$$\begin{aligned}\int d^4x(\mathcal{L} + J\Phi) = \int d^4\,x(\mathcal{L}[\phi_c] + J\phi_c) + \int d^4x\,\eta(x)\left(\frac{\delta\mathcal{L}}{\delta\Phi} + J\right) \\ +\frac{1}{2}\int d^4x\, d^4y\,\eta(x)i\mathcal{D}^{-1}(\phi_c, x-y)\eta(y) + \dots\end{aligned} \tag{A.17}$$

with

$$\begin{aligned}i\mathcal{D}^{-1}(\phi_c, x-y) = \frac{\delta}{\delta\Phi(x)}\frac{\delta}{\delta\Phi(y)}\int d^4z[\mathcal{L}[\Phi] + J(z)\Phi(z)]|_{\Phi=\phi_c} \\ = [-\partial^2 - V''(\phi_c(x))]\delta^{(4)}(x-y)\end{aligned} \tag{A.18}$$

is the inverse propagator in configuration space evaluated at $\Phi = \phi_c$. Here the functional derivatives of $\mathcal{L}$ are evaluated at $\phi_{cl}(x)$. The linear term in η vanishes.

We keep only the quadratic term in η (the higher order terms represent perturbative corrections). This term is essentially a Gaussian integral. Therefore we can solve Eq. (A.2), using the invariance of the path integral measure $\mathcal{D}\Phi = \mathcal{D}\eta$ as follows:

$$e^{iW[J]} \simeq e^{i\int d^4x[\mathcal{L}(\phi_c)+J(\phi_c)]} \int \mathcal{D}\eta \exp\left(\frac{i}{2}\int d^4x d^4y \eta(x) i\mathcal{D}^{-1}(\phi_c, x-y)\eta(y)\right)$$
$$= \mathcal{N} e^{i\int d^4x[\mathcal{L}(\phi_c)+J(\phi_c)]} [\det i\mathcal{D}^{-1}(\phi_c, x-y)]^{-1/2} \tag{A.19}$$

up to an irrelevant renormalization constant $\mathcal{N}$. By replacing Eq.(A.19) in the definition of the effective action, Eq. (A.6) , we obtain:

$$\Gamma[\phi_c] = S[\phi_{cl}] + \frac{i}{2}\log \det \mathcal{D}^{-1}(\phi_c, x-y) \tag{A.20}$$

where

$$S[\phi_c] = \int d^4x\, \mathcal{L}(\phi_c, \partial_\mu \phi_c) \tag{A.21}$$

The effective potential is obtained by evaluating (A.20) for a space-time independent classical field configuration, that here we denote with ϕ_c:

$$-\mathcal{V}_4 V_{\text{eff}}(\phi_c) = -\mathcal{V}_4 V_0(\phi_c) + \frac{i}{2}\log \det i\mathcal{D}^{-1}(\phi_c, x-y) \tag{A.22}$$

with $-\mathcal{V}_4 \equiv \int d^4x$ ad the space-time volume, that stems from the fact that ϕ_c is space-time independent. Moreover, the homogeniety of ϕ_c allows us to use the following identity:

$$\log \det i\mathcal{D}^{-1}(\phi_c, x-y) = \text{tr } \log\ i\mathcal{D}^{-1}(\phi_c, x-y) \tag{A.23}$$

We evaluate the functional trace, denoted by tr, by setting $x = y$ and integrating over the space-time. This gives:

$$\log\ \det i\mathcal{D}^{-1}(\phi_c, x-y) = \mathcal{V}_4 \log\ i\mathcal{D}^{-1}(\phi_c, 0) = \mathcal{V}_4 \int \frac{d^4\,k}{(2\pi)^4} \log i\tilde{\mathcal{D}}^{-1}(\phi_c, k) \tag{A.24}$$

where $\tilde{\mathcal{D}}^{-1}(\phi_c, k)$ denotes the four-dimensional Fourier transform of $\mathcal{D}^{-1}(\phi_c, x-y)$.

For a generic quantum field theory, where have a number n of fields interacting with Φ, the formula for the one-loop effective potential is given by:

$$V_{\text{eff}}(\phi) = V_0(\phi) + i\sum_n \eta_n \int \frac{d^4\,k}{(2\pi)^4} \text{Tr } \log\ i\tilde{\mathcal{D}}^{-1}(\phi_c, k) \tag{A.25}$$

The trace acts on all internal indices,i.e. Lorentz or gauge and therefore we use the symbol Tr to distinguish it from the functional trace tr. The factor η_n is the power of the functional determinant from the gaussisan path integral and it is given by:

$$\eta_n = \begin{cases} -\frac{1}{2} & \text{bosonic fields} \\ +1 & \text{fermionic fields} \end{cases} \tag{A.26}$$

A.1.2 U(1)' phase transition

Now we are going to compute the one-loop effective potential for our model using the background field method. The relevant terms in the Lagrangian are:

$$\mathcal{L} = \mathcal{L}_\phi + \mathcal{L}_{A'} \tag{A.27}$$

with:

$$\mathcal{L}_\phi = (D_\mu \phi)^\dagger (D_\mu \phi) - \lambda_\phi \phi^4 \tag{A.28}$$

$$\mathcal{L}_{A'} = -\frac{1}{4} F'_{\mu\nu} F'^{\mu\nu} \tag{A.29}$$

where ϕ is the dark Higgs scalar, $F'_{\mu\nu} = \partial_\mu A'_\nu - \partial_\nu A'_\mu$ is the field strength tensor of the $U(1)'$ gauge symmetry, with associated gauge boson A'_μ and the covariant derivative $D_\mu = \partial_\mu - ig' A'_\mu$. We notice that:

$$\begin{aligned} -\frac{1}{4}(\partial_\mu A'_\nu - \partial_\nu A'_\mu)(\partial^\mu A'^\nu - \partial^\nu A'^\mu) = -\frac{1}{4}(&\partial_\mu A'_\nu \partial^\mu A'^\nu - \partial_\mu A'_\nu \partial^\nu A'^\mu \\ &-\partial_\nu A'_\mu \partial^\mu A'^\nu + \partial_\nu A'_\mu \partial^\nu A'^\mu) \end{aligned} \tag{A.30}$$

which, by integrating by parts, can be rewritten as follows:

$$\mathcal{L}_{A'} = -\frac{1}{2}[A'^\mu (g_{\mu\nu}\partial^2 - \partial_\mu \partial_\nu) A'^\nu] \tag{A.31}$$

Let the background value of the complex scalar be ϕ_c. By the assumption of Poincarè symmetry, ϕ_c must be a constant. For the same reason, the background value of the vector field A'_μ must vanish. Then we have:

$$\phi = \frac{\varphi_r(x) + i\varphi_i(x) + \phi_c}{\sqrt{2}} \tag{A.32}$$

where $\varphi_r(x), \varphi_i(x)$ and $A'_\mu(x)$ are the fluctuating fields. In the following, the space-time dependence of the these fields will be implicit. Performing the shift given by eq. (A.32) and keeping only the quadratic terms, after a straightforward computation, we obtain:

$$\mathcal{L}^{(2)} = \frac{1}{2} A'_\mu (g^{\mu\nu}\partial^2 + g'^2 \phi_c^2 - \partial^\mu \partial^\nu) A'_\nu + \frac{1}{2}\varphi_r(-\partial^2 - 3\lambda\phi^2)\varphi_r + \frac{1}{2}\varphi_i(-\partial^2 - \lambda\phi^2)\varphi_i \tag{A.33}$$

We immediately read off the expressions of the field dpeendents masses:

$$m^2_{A'}(\phi) = g^{'2}\phi_c^2 \tag{A.34}$$

$$m^2_{\varphi_i}(\phi) = \lambda\phi_c^2 \tag{A.35}$$

$$m^2_{\varphi_r}(\phi) = 3\lambda\phi_c^2 \tag{A.36}$$

and, as described in the previous section, the expression of the inverse propagators in momentum space are given by:

$$i\tilde{D}_k^{-1} = -k^2 + m_k^2(\phi) \tag{A.37}$$

where $k = \{\varphi_i, \varphi_r, A\}$ identifies the field. To solve the integral in momentum space of Eq. (A.25), we work in *dimensional regularization* with $d = 4 - 2\epsilon$. We have to solve integrals of the form:

$$-\frac{i}{2}\mu^{2\epsilon}\int \frac{d^dk}{(2\pi)^d}\log\left[-k^2 + m^2(\phi)\right] \tag{A.38}$$

where μ is a mass parameter introduced to keep the correct dimension of the potential [1]. This loop integral can evaluated after a Wick rotation (see for example Ref. [135]),giving the following result:

$$-\frac{i}{2}\mu^{2\epsilon}\int \frac{d^dk}{(2\pi)^d}\log\left[-k^2 + m^2(\phi)\right] = \frac{1}{4}\frac{m^2(\phi)}{(4\pi)^2}\left(\log\frac{m^2(\phi)}{\mu^2} - \frac{3}{2} - \Delta_\epsilon\right) \tag{A.39}$$

where we have introduced the *modified minimal subtraction* ($\overline{\text{MS}}$) term:

$$\Delta_\epsilon = \frac{1}{\epsilon} - \gamma_E + \log 4\pi \tag{A.40}$$

with γ_E is Euler-Mascheroni constant. After the ϵ-expansion and the renormalization in the $\overline{\text{MS}}$ scheme, taking into account the degrees of freedom of each field $n_k = \{1, 1, 3\}$, the one-loop contribution to the effective potential reads:

$$\begin{aligned} V^{(1)}_{eff}(\phi_c) = \frac{1}{64\pi^2}\Bigg[3m_{A'}(\phi_c)^4\left(\log\frac{m^2_{A'}(\phi_c)}{M^2} - \frac{5}{6}\right) \\ +m_r^4(\phi_c)\left(\log\frac{m_r^2(\phi_c)}{M^2} - \frac{3}{2}\right) + m_i^4(\phi_c)\left(\log\frac{m_i^2(\phi_c)}{M^2} - \frac{3}{2}\right)\Bigg] \end{aligned} \tag{A.41}$$

[1] In the main text the scale μ is denoted as M, to distinguish it from the trilinear coupling in the UV model

Bibliography

[1] Georges Aad et al. "Observation of a new particle in the search for the Standard Model Higgs boson with the ATLAS detector at the LHC". In: *Phys. Lett. B* 716 (2012), pp. 1–29. DOI: 10.1016/j.physletb.2012.08.020. arXiv: 1207.7214 [hep-ex].

[2] Serguei Chatrchyan et al. "Observation of a New Boson at a Mass of 125 GeV with the CMS Experiment at the LHC". In: *Phys. Lett. B* 716 (2012), pp. 30–61. DOI: 10.1016/j.physletb.2012.08.021. arXiv: 1207.7235 [hep-ex].

[3] Antonio Riotto. "Theories of baryogenesis". In: *ICTP Summer School in High-Energy Physics and Cosmology*. July 1998, pp. 326–436. arXiv: hep-ph/9807454.

[4] A. D. Sakharov. "Violation of CP Invariance, C asymmetry, and baryon asymmetry of the universe". In: *Pisma Zh. Eksp. Teor. Fiz.* 5 (1967), pp. 32–35. DOI: 10.1070/PU1991v034n05ABEH002497.

[5] Gilly Elor et al. "New Ideas in Baryogenesis: A Snowmass White Paper". In: *Snowmass 2021*. Mar. 2022. arXiv: 2203.05010 [hep-ph].

[6] J. L. Barrow et al. "Theories and Experiments for Testable Baryogenesis Mechanisms: A Snowmass White Paper". In: (Mar. 2022). arXiv: 2203.07059 [hep-ph].

[7] B. P. Abbott et al. "Observation of Gravitational Waves from a Binary Black Hole Merger". In: *Phys. Rev. Lett.* 116.6 (2016), p. 061102. DOI: 10.1103/PhysRevLett.116.061102. arXiv: 1602.03837 [gr-qc].

[8] Pierre Auclair et al. "Cosmology with the Laser Interferometer Space Antenna". In: *Living Rev. Rel.* 26.1 (2023), p. 5. DOI: 10.1007/s41114-023-00045-2. arXiv: 2204.05434 [astro-ph.CO].

[9] Andrey Katz and Antonio Riotto. "Baryogenesis and Gravitational Waves from Runaway Bubble Collisions". In: *JCAP* 11 (2016), p. 011. DOI: 10.1088/1475-7516/2016/11/011. arXiv: 1608.00583 [hep-ph].

[10] Iason Baldes et al. “Baryogenesis via relativistic bubble expansion”. In: *Phys. Rev. D* 104.11 (2021), p. 115029. DOI: 10.1103/PhysRevD.104.115029. arXiv: 2106.15602 [hep-ph].

[11] Aleksandr Azatov, Miguel Vanvlasselaer, and Wen Yin. “Baryogenesis via relativistic bubble walls”. In: *JHEP* 10 (2021), p. 043. DOI: 10.1007/JHEP10(2021)043. arXiv: 2106.14913 [hep-ph].

[12] Maximilian Dichtl et al. “Baryogenesis and leptogenesis from supercooled confinement”. In: *JHEP* 02 (2024), p. 059. DOI: 10.1007/JHEP02(2024)059. arXiv: 2312.09282 [hep-ph].

[13] Feryal Özel and Paulo Freire. “Masses, Radii, and the Equation of State of Neutron Stars”. In: *Ann. Rev. Astron. Astrophys.* 54 (2016), pp. 401–440. DOI: 10.1146/annurev-astro-081915-023322. arXiv: 1603.02698 [astro-ph.HE].

[14] John G. Hartnett and Andre Luiten. “Colloquium: Comparison of Astrophysical and Terrestrial Frequency Standards”. In: *Rev. Mod. Phys.* 83 (2011), pp. 1–9. DOI: 10.1103/RevModPhys.83.1. arXiv: 1004.0115 [astro-ph.IM].

[15] Gerard Auger and Eric Plagnol, eds. *An Overview of Gravitational Waves: Theory, Sources and Detection*. Singapore: World Scientific, 2017. ISBN: 978-981-314-175-9, 978-981-314-177-3. DOI: 10.1142/10082.

[16] Gabriella Agazie et al. “The NANOGrav 15 yr Data Set: Evidence for a Gravitational-wave Background”. In: *Astrophys. J. Lett.* 951.1 (2023), p. L8. DOI: 10.3847/2041-8213/acdac6. arXiv: 2306.16213 [astro-ph.HE].

[17] Daniel J. Reardon et al. “Search for an Isotropic Gravitational-wave Background with the Parkes Pulsar Timing Array”. In: *Astrophys. J. Lett.* 951.1 (2023), p. L6. DOI: 10.3847/2041-8213/acdd02. arXiv: 2306.16215 [astro-ph.HE].

[18] J. Antoniadis et al. “The second data release from the European Pulsar Timing Array - III. Search for gravitational wave signals”. In: *Astron. Astrophys.* 678 (2023), A50. DOI: 10.1051/0004-6361/202346844. arXiv: 2306.16214 [astro-ph.HE].

[19] Heng Xu et al. “Searching for the Nano-Hertz Stochastic Gravitational Wave Background with the Chinese Pulsar Timing Array Data Release I”. In: *Res. Astron. Astrophys.* 23.7 (2023), p. 075024. DOI: 10.1088/1674-4527/acdfa5. arXiv: 2306.16216 [astro-ph.HE].

[20] Bence Bécsy, Neil J. Cornish, and Luke Zoltan Kelley. "Exploring Realistic Nanohertz Gravitational-wave Backgrounds". In: *Astrophys. J.* 941.2 (2022), p. 119. DOI: 10.3847/1538-4357/aca1b2. arXiv: 2207.01607 [astro-ph.HE].

[21] Zaven Arzoumanian et al. "Searching for Gravitational Waves from Cosmological Phase Transitions with the NANOGrav 12.5-Year Dataset". In: *Phys. Rev. Lett.* 127.25 (2021), p. 251302. DOI: 10.1103/PhysRevLett.127.251302. arXiv: 2104.13930 [astro-ph.CO].

[22] Simone Blasi, Vedran Brdar, and Kai Schmitz. "Has NANOGrav found first evidence for cosmic strings?" In: *Phys. Rev. Lett.* 126.4 (2021), p. 041305. DOI: 10.1103/PhysRevLett.126.041305. arXiv: 2009.06607 [astro-ph.CO].

[23] Ricardo Z. Ferreira et al. "Gravitational waves from domain walls in Pulsar Timing Array datasets". In: *JCAP* 02 (2023), p. 001. DOI: 10.1088/1475-7516/2023/02/001. arXiv: 2204.04228 [astro-ph.CO].

[24] Wolfram Ratzinger and Pedro Schwaller. "Whispers from the dark side: Confronting light new physics with NANOGrav data". In: *SciPost Phys.* 10.2 (2021), p. 047. DOI: 10.21468/SciPostPhys.10.2.047. arXiv: 2009.11875 [astro-ph.CO].

[25] Deng Wang. "Novel Physics with International Pulsar Timing Array: Axionlike Particles, Domain Walls and Cosmic Strings". In: (Mar. 2022). arXiv: 2203.10959 [astro-ph.CO].

[26] Virgile Dandoy, Valerie Domcke, and Fabrizio Rompineve. "Search for scalar induced gravitational waves in the international pulsar timing array data release 2 and NANOgrav 12.5 years datasets". In: *SciPost Phys. Core* 6 (2023), p. 060. DOI: 10.21468/SciPostPhysCore.6.3.060. arXiv: 2302.07901 [astro-ph.CO].

[27] Adeela Afzal et al. "The NANOGrav 15 yr Data Set: Search for Signals from New Physics". In: *Astrophys. J. Lett.* 951.1 (2023), p. L11. DOI: 10.3847/2041-8213/acdc91. arXiv: 2306.16219 [astro-ph.HE].

[28] Paul A. M. Dirac. "The quantum theory of the electron". In: *Proc. Roy. Soc. Lond. A* 117 (1928), pp. 610–624. DOI: 10.1098/rspa.1928.0023.

[29] C. D. Anderson. "The Positive Electron". In: *Phys. Rev.* 43 (1933), pp. 491–494. DOI: 10.1103/PhysRev.43.491.

[30] Laurent Canetti, Marco Drewes, and Mikhail Shaposhnikov. "Matter and Antimatter in the Universe". In: *New J. Phys.* 14 (2012), p. 095012. DOI: 10.1088/1367-2630/14/9/095012. arXiv: 1204.4186 [hep-ph].

[31] Paolo Coppi. "How Do We know Antimater is Absent?" In: *eConf* C040802 (2004). Ed. by Joanne Hewett et al., p. L017.

[32] G. Steigman. "Observational tests of antimatter cosmologies". In: *Ann. Rev. Astron. Astrophys.* 14 (1976), pp. 339–372. DOI: 10.1146/annurev.aa.14.090176.002011.

[33] M. Aguilar et al. "The Alpha Magnetic Spectrometer (AMS) on the international space station: Part II — Results from the first seven years". In: *Phys. Rept.* 894 (2021), pp. 1–116. DOI: 10.1016/j.physrep.2020.09.003.

[34] Andrew G. Cohen, A. De Rujula, and S. L. Glashow. "A Matter - antimatter universe?" In: *Astrophys. J.* 495 (1998), pp. 539–549. DOI: 10.1086/305328. arXiv: astro-ph/9707087.

[35] Andrew G. Cohen and A. De Rujula. "Scars on the CBR?" In: (Sept. 1997). arXiv: astro-ph/9709132.

[36] Ryan J. Cooke, Max Pettini, and Charles C. Steidel. "One Percent Determination of the Primordial Deuterium Abundance". In: *Astrophys. J.* 855.2 (2018), p. 102. DOI: 10.3847/1538-4357/aaab53. arXiv: 1710.11129 [astro-ph.CO].

[37] Brian D. Fields. "The primordial lithium problem". In: *Ann. Rev. Nucl. Part. Sci.* 61 (2011), pp. 47–68. DOI: 10.1146/annurev-nucl-102010-130445. arXiv: 1203.3551 [astro-ph.CO].

[38] N. Aghanim et al. "Planck 2018 results. I. Overview and the cosmological legacy of Planck". In: *Astron. Astrophys.* 641 (2020), A1. DOI: 10.1051/0004-6361/201833880. arXiv: 1807.06205 [astro-ph.CO].

[39] John Ellis and David Wands. "Inflation (2023)". In: (Dec. 2023). arXiv: 2312.13238 [astro-ph.CO].

[40] Gordan Krnjaic. "Can the Baryon Asymmetry Arise From Initial Conditions?" In: *Phys. Rev. D* 96.3 (2017), p. 035041. DOI: 10.1103/PhysRevD.96.035041. arXiv: 1606.05344 [hep-ph].

[41] J. H. Christenson et al. "Evidence for the 2π Decay of the K_2^0 Meson". In: *Phys. Rev. Lett.* 13 (1964), pp. 138–140. DOI: 10.1103/PhysRevLett.13.138.

[42] Gerard 't Hooft. "Symmetry Breaking Through Bell-Jackiw Anomalies". In: *Phys. Rev. Lett.* 37 (1976). Ed. by Mikhail A. Shifman, pp. 8–11. DOI: 10.1103/PhysRevLett.37.8.

[43] V. A. Kuzmin, V. A. Rubakov, and M. E. Shaposhnikov. "On the Anomalous Electroweak Baryon Number Nonconservation in the Early Universe". In: *Phys. Lett. B* 155 (1985), p. 36. DOI: 10.1016/0370-2693(85)91028-7.

[44] Dietrich Bodeker and Wilfried Buchmuller. "Baryogenesis from the weak scale to the grand unification scale". In: *Rev. Mod. Phys.* 93.3 (2021), p. 035004. DOI: 10.1103/RevModPhys.93.035004. arXiv: 2009.07294 [hep-ph].

[45] K. Kajantie et al. "Is There a Hot Electroweak Phase Transition at m(H) larger or equal to m(W)"?" In: *Physical Review Letters* 77.14 (Sept. 1996), pp. 2887–2890. ISSN: 1079-7114. DOI: 10.1103/physrevlett.77.2887. URL: http://dx.doi.org/10.1103/PhysRevLett.77.2887.

[46] K. Rummukainen et al. "The universality class of the electroweak theory". In: *Nuclear Physics B* 532.1–2 (Oct. 1998), pp. 283–314. ISSN: 0550-3213. DOI: 10.1016/s0550-3213(98)00494-5. URL: http://dx.doi.org/10.1016/S0550-3213(98)00494-5.

[47] F. Csikor, Z. Fodor, and J. Heitger. "End Point of the Hot Electroweak Phase Transition". In: *Physical Review Letters* 82.1 (Jan. 1999), pp. 21–24. ISSN: 1079-7114. DOI: 10.1103/physrevlett.82.21. URL: http://dx.doi.org/10.1103/PhysRevLett.82.21.

[48] M. B. Gavela et al. "Standard model CP violation and baryon asymmetry". In: *Mod. Phys. Lett. A* 9 (1994), pp. 795–810. DOI: 10.1142/S0217732394000629. arXiv: hep-ph/9312215.

[49] M. B. Gavela et al. "Standard model CP violation and baryon asymmetry. Part 2: Finite temperature". In: *Nucl. Phys. B* 430 (1994), pp. 382–426. DOI: 10.1016/0550-3213(94)00410-2. arXiv: hep-ph/9406289.

[50] Björn Garbrecht. "Why is there more matter than antimatter? Calculational methods for leptogenesis and electroweak baryogenesis". In: *Prog. Part. Nucl. Phys.* 110 (2020), p. 103727. DOI: 10.1016/j.ppnp.2019.103727. arXiv: 1812.02651 [hep-ph].

[51] C. Jarlskog. "Commutator of the Quark Mass Matrices in the Standard Electroweak Model and a Measure of Maximal CP Nonconservation". In: *Phys. Rev. Lett.* 55 (1985), p. 1039. DOI: 10.1103/PhysRevLett.55.1039.

[52] Michael Dine and Alexander Kusenko. "The Origin of the matter - antimatter asymmetry". In: *Rev. Mod. Phys.* 76 (2003), p. 1. DOI: 10.1103/RevModPhys.76.1. arXiv: hep-ph/0303065.

[53] James M. Cline. "Baryogenesis". In: *Les Houches Summer School - Session 86: Particle Physics and Cosmology: The Fabric of Spacetime*. Sept. 2006. arXiv: hep-ph/0609145.

[54] Djuna Croon et al. "GUT Physics in the era of the LHC". In: *Front. in Phys.* 7 (2019), p. 76. DOI: 10.3389/fphy.2019.00076. arXiv: 1903.04977 [hep-ph].

[55] Yann Gouttenoire. *Beyond the Standard Model Cocktail*. Springer Theses. Cham: Springer, 2022. ISBN: 978-3-031-11862-3, 978-3-031-11861-6. DOI: 10.1007/978-3-031-11862-3. arXiv: 2207.01633 [hep-ph].

[56] Sebastian Bruggisser et al. "Electroweak Phase Transition and Baryogenesis in Composite Higgs Models". In: *JHEP* 12 (2018), p. 099. DOI: 10.1007/JHEP12(2018)099. arXiv: 1804.07314 [hep-ph].

[57] Iason Baldes, Thomas Konstandin, and Geraldine Servant. "A first-order electroweak phase transition from varying Yukawas". In: *Phys. Lett. B* 786 (2018), pp. 373–377. DOI: 10.1016/j.physletb.2018.10.015. arXiv: 1604.04526 [hep-ph].

[58] Sebastian A. R. Ellis, Seyda Ipek, and Graham White. "Electroweak Baryogenesis from Temperature-Varying Couplings". In: *JHEP* 08 (2019), p. 002. DOI: 10.1007/JHEP08(2019)002. arXiv: 1905.11994 [hep-ph].

[59] M. Fukugita and T. Yanagida. "Baryogenesis Without Grand Unification". In: *Phys. Lett. B* 174 (1986), pp. 45–47. DOI: 10.1016/0370-2693(86)91126-3.

[60] Alessandro Granelli. "Standard and Non-Standard Aspects of Neutrino Physics". In: *Universe* 10.4 (2024), p. 164. DOI: 10.3390/universe10040164. arXiv: 2403.16308 [hep-ph].

[61] Heinz Pagels and Joel R. Primack. "Supersymmetry, Cosmology and New TeV Physics". In: *Phys. Rev. Lett.* 48 (1982), p. 223. DOI: 10.1103/PhysRevLett.48.223.

[62] Steven Weinberg. "Cosmological Constraints on the Scale of Supersymmetry Breaking". In: *Phys. Rev. Lett.* 48 (1982), p. 1303. DOI: 10.1103/PhysRevLett.48.1303.

[63] Tom Banks, David B. Kaplan, and Ann E. Nelson. "Cosmological implications of dynamical supersymmetry breaking". In: *Phys. Rev. D* 49 (1994), pp. 779–787. DOI: 10.1103/PhysRevD.49.779. arXiv: hep-ph/9308292.

[64] Pierre Sikivie. "Axion Cosmology". In: *Lect. Notes Phys.* 741 (2008). Ed. by Markus Kuster, Georg Raffelt, and Berta Beltran, pp. 19–50. DOI: 10.1007/978-3-540-73518-2_2. arXiv: astro-ph/0610440.

[65] Nima Arkani-Hamed, Massimo Porrati, and Lisa Randall. "Holography and phenomenology". In: *Journal of High Energy Physics* 2001.08 (Aug. 2001), pp. 017–017. ISSN: 1029-8479. DOI: 10.1088/1126-6708/2001/08/017. URL: http://dx.doi.org/10.1088/1126-6708/2001/08/017.

[66] Mark Claudson, Lawrence J. Hall, and Ian Hinchliffe. "COSMOLOGICAL BARYON GENERATION AT LOW TEMPERATURES". In: *Nucl. Phys. B* 241 (1984), pp. 309–332. DOI: 10.1016/0550-3213(84)90212-8.

[67] Savas Dimopoulos and Lawrence J. Hall. "Baryogenesis at the MeV Era". In: *Phys. Lett. B* 196 (1987), pp. 135–141. DOI: 10.1016/0370-2693(87)90593-4.

[68] Torsten Bringmann, James M. Cline, and Jonathan M. Cornell. "Baryogenesis from neutron-dark matter oscillations". In: *Phys. Rev. D* 99.3 (2019), p. 035024. DOI: 10.1103/PhysRevD.99.035024. arXiv: 1810.08215 [hep-ph].

[69] Akshay Ghalsasi, David McKeen, and Ann E. Nelson. "Baryogenesis via Mesino Oscillations". In: *Phys. Rev. D* 92.7 (2015), p. 076014. DOI: 10.1103/PhysRevD.92.076014. arXiv: 1508.05392 [hep-ph].

[70] Gilly Elor, Miguel Escudero, and Ann Nelson. "Baryogenesis and Dark Matter from B Mesons". In: *Phys. Rev. D* 99.3 (2019), p. 035031. DOI: 10.1103/PhysRevD.99.035031. arXiv: 1810.00880 [hep-ph].

[71] Gilly Elor and Robert McGehee. "Making the Universe at 20 MeV". In: *Phys. Rev. D* 103.3 (2021), p. 035005. DOI: 10.1103/PhysRevD.103.035005. arXiv: 2011.06115 [hep-ph].

[72] Fatemeh Elahi, Gilly Elor, and Robert McGehee. "Charged B mesogenesis". In: *Phys. Rev. D* 105.5 (2022), p. 055024. DOI: 10.1103/PhysRevD.105.055024. arXiv: 2109.09751 [hep-ph].

[73] D. A. Kirzhnits and Andrei D. Linde. "Macroscopic Consequences of the Weinberg Model". In: *Phys. Lett. B* 42 (1972), pp. 471–474. DOI: 10.1016/0370-2693(72)90109-8.

[74] M. A. Stephanov. "QCD phase diagram: An Overview". In: *PoS* LAT2006 (2006). Ed. by Tom Blum et al., p. 024. DOI: 10.22323/1.032.0024. arXiv: hep-lat/0701002.

[75] Sidney R. Coleman. "The Fate of the False Vacuum. 1. Semiclassical Theory". In: *Phys. Rev. D* 15 (1977). [Erratum: Phys.Rev.D 16, 1248 (1977)], pp. 2929–2936. DOI: 10.1103/PhysRevD.16.1248.

[76] Curtis G. Callan and Sidney Coleman. "Fate of the false vacuum. II. First quantum corrections". In: *Phys. Rev. D* 16 (6 Sept. 1977), pp. 1762–1768. DOI: 10.1103/PhysRevD.16.1762. URL: https://link.aps.org/doi/10.1103/PhysRevD.16.1762.

[77] Andrei D. Linde. "Fate of the False Vacuum at Finite Temperature: Theory and Applications". In: *Phys. Lett. B* 100 (1981), pp. 37–40. DOI: 10.1016/0370-2693(81)90281-1.

[78] Andrei D. Linde. "Decay of the False Vacuum at Finite Temperature". In: *Nucl. Phys. B* 216 (1983). [Erratum: Nucl.Phys.B 223, 544 (1983)], p. 421. DOI: 10.1016/0550-3213(83)90072-X.

[79] Greg W. Anderson and Lawrence J. Hall. "The Electroweak phase transition and baryogenesis". In: *Phys. Rev. D* 45 (1992), pp. 2685–2698. DOI: 10.1103/PhysRevD.45.2685.

[80] Germano Nardini, Mariano Quirós, and Andrea Wulzer. "A confining strong first-order electroweak phase transition". In: *Journal of High Energy Physics* 2007.09 (Sept. 2007), pp. 077–077. ISSN: 1029-8479. DOI: 10.1088/1126-6708/2007/09/077. URL: http://dx.doi.org/10.1088/1126-6708/2007/09/077.

[81] Mark B. Hindmarsh et al. "Phase transitions in the early universe". In: *SciPost Phys. Lect. Notes* 24 (2021), p. 1. DOI: 10.21468/SciPostPhysLectNotes.24. arXiv: 2008.09136 [astro-ph.CO].

[82] Iason Baldes et al. "Particle shells from relativistic bubble walls". In: (Mar. 2024). arXiv: 2403.05615 [hep-ph].

[83] Thomas Konstandin and Géraldine Servant. "Cosmological consequences of nearly conformal dynamics at the TeV scale". In: *Journal of Cosmology and Astroparticle Physics* 2011.12 (Dec. 2011), pp. 009–009. ISSN: 1475-7516. DOI: 10.1088/1475-7516/2011/12/009. URL: http://dx.doi.org/10.1088/1475-7516/2011/12/009.

[84] Lisa Randall and Géraldine Servant. "Gravitational waves from warped spacetime". In: *Journal of High Energy Physics* 2007.05 (May 2007), pp. 054–054. ISSN: 1029-8479. DOI: 10.1088/1126-6708/2007/05/054. URL: http://dx.doi.org/10.1088/1126-6708/2007/05/054.

[85] Thomas Hambye, Alessandro Strumia, and Daniele Teresi. "Super-cool Dark Matter". In: *Journal of High Energy Physics* 2018.8 (Aug. 2018). ISSN: 1029-8479. DOI: 10.1007/jhep08(2018)188. URL: http://dx.doi.org/10.1007/JHEP08(2018)188.

[86] Tiago Barreiro et al. "Some aspects of thermal inflation: The finite temperature potential and topological defects". In: *Physical Review D* 54.2 (July 1996), pp. 1379–1392. ISSN: 1089-4918. DOI: 10.1103/physrevd.54.1379. URL: http://dx.doi.org/10.1103/PhysRevD.54.1379.

[87] Richard Easther et al. "Thermal inflation and the gravitational wave background". In: *Journal of Cosmology and Astroparticle Physics* 2008.05 (May 2008), p. 013. ISSN: 1475-7516. DOI: 10.1088/1475-7516/2008/05/013. URL: http://dx.doi.org/10.1088/1475-7516/2008/05/013.

[88] Christophe Grojean, Géraldine Servant, and James D. Wells. "First-order electroweak phase transition in the standard model with a low cutoff". In: *Physical Review D* 71.3 (Feb. 2005). ISSN: 1550-2368. DOI: 10.1103/physrevd.71.036001. URL: http://dx.doi.org/10.1103/PhysRevD.71.036001.

[89] Mariano Quiros. "Finite temperature field theory and phase transitions". In: *ICTP Summer School in High-Energy Physics and Cosmology*. Jan. 1999, pp. 187–259. arXiv: hep-ph/9901312.

[90] Sidney R. Coleman and Erick J. Weinberg. "Radiative Corrections as the Origin of Spontaneous Symmetry Breaking". In: *Phys. Rev. D* 7 (1973), pp. 1888–1910. DOI: 10.1103/PhysRevD.7.1888.

[91] Cedric Delaunay, Christophe Grojean, and James D. Wells. "Dynamics of Non-renormalizable Electroweak Symmetry Breaking". In: *JHEP* 04 (2008), p. 029. DOI: 10.1088/1126-6708/2008/04/029. arXiv: 0711.2511 [hep-ph].

[92] L. Dolan and R. Jackiw. "Symmetry behavior at finite temperature". In: *Phys. Rev. D* 9 (12 June 1974), pp. 3320–3341. DOI: 10.1103/PhysRevD.9.3320. URL: https://link.aps.org/doi/10.1103/PhysRevD.9.3320.

[93] M. E. Carrington. "Effective potential at finite temperature in the standard model". In: *Phys. Rev. D* 45 (8 Apr. 1992), pp. 2933–2944. DOI: 10.1103/PhysRevD.45.2933. URL: https://link.aps.org/doi/10.1103/PhysRevD.45.2933.

[94] John Ellis, Marek Lewicki, and José Miguel No. "On the Maximal Strength of a First-Order Electroweak Phase Transition and its Gravitational Wave Signal". In: *JCAP* 04 (2019), p. 003. DOI: 10.1088/1475-7516/2019/04/003. arXiv: 1809.08242 [hep-ph].

[95] Sebastian Bruggisser et al. *Electroweak Phase Transition and Baryogenesis in Composite Higgs Models*. 2018. arXiv: 1804.07314 [hep-ph].

[96] Iason Baldes et al. "Supercool composite Dark Matter beyond 100 TeV". In: *Journal of High Energy Physics* 2022.7 (July 2022). ISSN: 1029-8479. DOI: 10.1007/jhep07(2022)084. URL: http://dx.doi.org/10.1007/JHEP07(2022)084.

[97] Walter D. Goldberger, Benjamín Grinstein, and Witold Skiba. "Distinguishing the Higgs Boson from the Dilaton at the Large Hadron Collider". In: *Physical Review Letters* 100.11 (Mar. 2008). ISSN: 1079-7114. DOI: 10.1103/physrevlett.100.111802. URL: http://dx.doi.org/10.1103/PhysRevLett.100.111802.

[98] Juan Maldacena. In: *International Journal of Theoretical Physics* 38.4 (1999), pp. 1113–1133. ISSN: 0020-7748. DOI: 10.1023/a:1026654312961. URL: http://dx.doi.org/10.1023/A:1026654312961.

[99] Lisa Randall and Raman Sundrum. "A Large mass hierarchy from a small extra dimension". In: *Phys. Rev. Lett.* 83 (1999), pp. 3370–3373. DOI: 10.1103/PhysRevLett.83.3370. arXiv: hep-ph/9905221.

[100] Riccardo Rattazzi and Alberto Zaffaroni. "Comments on the Holographic Picture of the Randall-Sundrum Model". In: *Journal of High Energy Physics* 2001.04 (Apr. 2001), pp. 021–021. ISSN: 1029-8479. DOI: 10.1088/1126-6708/2001/04/021. URL: http://dx.doi.org/10.1088/1126-6708/2001/04/021.

[101] Edward Witten. "Baryons in the 1/n Expansion". In: *Nucl. Phys. B* 160 (1979), pp. 57–115. DOI: 10.1016/0550-3213(79)90232-3.

[102] S. S. Gubser, I. R. Klebanov, and A. W. Peet. "Entropy and temperature of black 3-branes". In: *Physical Review D* 54.6 (Sept. 1996), pp. 3915–3919. ISSN: 1089-4918. DOI: 10.1103/physrevd.54.3915. URL: http://dx.doi.org/10.1103/PhysRevD.54.3915.

[103] Luigi Delle Rose et al. *Gravitational Waves from Supercool Axions*. 2020. arXiv: 1912.06139 [hep-ph].

[104] Federica Devoto et al. "False vacuum decay: an introductory review". In: *J. Phys. G* 49.10 (2022), p. 103001. DOI: 10.1088/1361-6471/ac7f24. arXiv: 2205.03140 [hep-ph].

[105] N. Aghanim et al. "Planck 2018 results. VI. Cosmological parameters". In: *Astron. Astrophys.* 641 (2020). [Erratum: Astron.Astrophys. 652, C4 (2021)], A6. DOI: 10.1051/0004-6361/201833910. arXiv: 1807.06209 [astro-ph.CO].

[106] Kalliopi Petraki and Raymond R. Volkas. "Review of asymmetric dark matter". In: *Int. J. Mod. Phys. A* 28 (2013), p. 1330028. DOI: 10.1142/S0217751X13300287. arXiv: 1305.4939 [hep-ph].

[107] Bartosz Fornal and Benjamin Grinstein. "Dark Matter Interpretation of the Neutron Decay Anomaly". In: *Phys. Rev. Lett.* 120.19 (2018). [Erratum: Phys.Rev.Lett. 124, 219901 (2020)], p. 191801. DOI: 10.1103/PhysRevLett.120.191801. arXiv: 1801.01124 [hep-ph].

[108] F. E. Wietfeldt. "The Neutron Lifetime". In: *8th International Workshop on the CKM Unitarity Triangle*. Nov. 2014. arXiv: 1411.3687 [nucl-ex].

[109] James M. Cline and Jonathan M. Cornell. "Dark decay of the neutron". In: *JHEP* 07 (2018), p. 081. DOI: 10.1007/JHEP07(2018)081. arXiv: 1803.04961 [hep-ph].

[110] Kyle Aitken et al. "Baryogenesis from Oscillations of Charmed or Beautiful Baryons". In: *Phys. Rev. D* 96.7 (2017), p. 075009. DOI: 10.1103/PhysRevD.96.075009. arXiv: 1708.01259 [hep-ph].

[111] C. Antel et al. "Feebly-interacting particles: FIPs 2022 Workshop Report". In: *Eur. Phys. J. C* 83.12 (2023), p. 1122. DOI: 10.1140/epjc/s10052-023-12168-5. arXiv: 2305.01715 [hep-ph].

[112] F. Petricca et al. "First results on low-mass dark matter from the CRESST-III experiment". In: *J. Phys. Conf. Ser.* 1342.1 (2020). Ed. by Ken Clark et al., p. 012076. DOI: 10.1088/1742-6596/1342/1/012076. arXiv: 1711.07692 [astro-ph.CO].

[113] J. D. Bjorken et al. "Search for Neutral Metastable Penetrating Particles Produced in the SLAC Beam Dump". In: *Phys. Rev. D* 38 (1988), p. 3375. DOI: 10.1103/PhysRevD.38.3375.

[114] Sarah Andreas, Carsten Niebuhr, and Andreas Ringwald. "New Limits on Hidden Photons from Past Electron Beam Dumps". In: *Phys. Rev. D* 86 (2012), p. 095019. DOI: 10.1103/PhysRevD.86.095019. arXiv: 1209.6083 [hep-ph].

[115] Jae Hyeok Chang, Rouven Essig, and Samuel D. McDermott. "Revisiting Supernova 1987A Constraints on Dark Photons". In: *JHEP* 01 (2017), p. 107. DOI: 10.1007/JHEP01(2017)107. arXiv: 1611.03864 [hep-ph].

[116] H. Leutwyler and Andrei V. Smilga. "NUCLEONS AT FINITE TEMPERATURE". In: *Nucl. Phys. B* 342 (1990), pp. 302–316. DOI: 10.1016/0550-3213(90)90192-G.

[117] V. L. Eletsky and B. L. Ioffe. "On the thermal mass shift of nucleons". In: *Phys. Lett. B* 401 (1997), pp. 327–329. DOI: 10.1016/S0370-2693(97)00417-6. arXiv: hep-ph/9702388.

[118] Paulo F. Bedaque. "Chiral perturbation theory analysis of baryon temperature mass shifts". In: *Phys. Lett. B* 387 (1996), pp. 1–8. DOI: 10.1016/0370-2693(96)00985-9. arXiv: hep-ph/9511365.

[119] Dirk Notzold and Georg Raffelt. "Neutrino dispersion at finite temperature and density". In: *Nucl. Phys. B* 307 (1988), pp. 924–936. DOI: 10.1016/0550-3213(88)90113-7.

[120] Nadia Fettes, Ulf-G. Meissner, and Sven Steininger. "Pion - nucleon scattering in chiral perturbation theory. 1. Isospin symmetric case". In: *Nucl. Phys. A* 640 (1998), pp. 199–234. DOI: 10.1016/S0375-9474(98)00452-7. arXiv: hep-ph/9803266.

[121] Jacobo Ruiz de Elvira et al. "Extracting the σ-term from low-energy pion-nucleon scattering". In: *J. Phys. G* 45.2 (2018), p. 024001. DOI: 10.1088/1361-6471/aa9422. arXiv: 1706.01465 [hep-ph].

[122] Marco Cirelli et al. "Consequences of DM/antiDM Oscillations for Asymmetric WIMP Dark Matter". In: *JCAP* 03 (2012), p. 015. DOI: 10.1088/1475-7516/2012/03/015. arXiv: 1110.3809 [hep-ph].

[123] Sean Tulin, Hai-Bo Yu, and Kathryn M. Zurek. "Oscillating Asymmetric Dark Matter". In: *JCAP* 05 (2012), p. 013. DOI: 10.1088/1475-7516/2012/05/013. arXiv: 1202.0283 [hep-ph].

[124] Z. Tang et al. "Search for the Neutron Decay n$\rightarrow$ X+γ where X is a dark matter particle". In: *Phys. Rev. Lett.* 121.2 (2018), p. 022505. DOI: 10.1103/PhysRevLett.121.022505. arXiv: 1802.01595 [nucl-ex].

[125] Georges Aad et al. "Search for squarks and gluinos in final states with jets and missing transverse momentum using 139 fb^{-1} of $\sqrt{s}$ =13 TeV pp collision data with the ATLAS detector". In: *JHEP* 02 (2021), p. 143. DOI: 10.1007/JHEP02(2021)143. arXiv: 2010.14293 [hep-ex].

[126] Yasumichi Aoki et al. "Improved lattice computation of proton decay matrix elements". In: *Phys. Rev. D* 96.1 (2017), p. 014506. DOI: 10.1103/PhysRevD.96.014506. arXiv: 1705.01338 [hep-lat].

[127] Edward Witten. "Cosmological Consequences of a Light Higgs Boson". In: *Nucl. Phys. B* 177 (1981), pp. 477–488. DOI: 10.1016/0550-3213(81)90182-6.

[128] Noam Levi, Toby Opferkuch, and Diego Redigolo. "The supercooling window at weak and strong coupling". In: *JHEP* 02 (2023), p. 125. DOI: 10.1007/JHEP02(2023)125. arXiv: 2212.08085 [hep-ph].

[129] Luigi Delle Rose et al. "Gravitational Waves from Supercool Axions". In: *JHEP* 04 (2020), p. 025. DOI: 10.1007/JHEP04(2020)025. arXiv: 1912.06139 [hep-ph].

[130] Yann Gouttenoire. "First-Order Phase Transition Interpretation of Pulsar Timing Array Signal Is Consistent with Solar-Mass Black Holes". In: *Phys. Rev. Lett.* 131.17 (2023), p. 171404. DOI: 10.1103/PhysRevLett.131.171404. arXiv: 2307.04239 [hep-ph].

[131] Martin Wolfgang Winkler and Katherine Freese. "Origin of the Stochastic Gravitational Wave Background: First-Order Phase Transition vs. Black Hole Mergers". In: (Jan. 2024). arXiv: 2401.13729 [astro-ph.CO].

[132] Torsten Bringmann et al. "Does NANOGrav observe a dark sector phase transition?" In: *JCAP* 11 (2023), p. 053. DOI: 10.1088/1475-7516/2023/11/053. arXiv: 2306.09411 [astro-ph.CO].

[133] Yang Bai and Mrunal Korwar. "Cosmological constraints on first-order phase transitions". In: *Phys. Rev. D* 105.9 (2022), p. 095015. DOI: 10.1103/PhysRevD.105.095015. arXiv: 2109.14765 [hep-ph].

[134] Shihao Deng and Ligong Bian. "Constraints on new physics around the MeV scale with cosmological observations". In: *Phys. Rev. D* 108.6 (2023), p. 063516. DOI: 10.1103/PhysRevD.108.063516. arXiv: 2304.06576 [hep-ph].

[135] Michael E. Peskin and Daniel V. Schroeder. *An Introduction to quantum field theory*. Reading, USA: Addison-Wesley, 1995. ISBN: 978-0-201-50397-5.